EUROPEAN ORGANIZATION FOR NUCLEAR RESEARCH

DIFFRACTION OF HADRONIC WAVES

U. Amaldi, M. Jacob and G. Matthiae

To be published in

Annual Review of Nuclear Science, Vol. 26, 1976

GENEVA 1976

Contents

1. INTRODUCTION

Most of the known fundamental particles are hadrons, particles with strong interactions, and evidence for their composite nature is now overwhelming. Indeed, hadrons are extended in space with typical dimensions of the order of 1 fm. This is the range of strong interactions. In a collision the centre of mass energy of two hadrons is thus concentrated, for a time of the order of 10^{-23} sec, in a small volume whose transverse dimensions are of the order of 1 fm. Strong interactions are such that, in collisions at centre of mass energies much larger than the proton rest mass, there are many possible final states which, in general, contain many newly produced hadrons. Since many inelastic interactions can occur, a non negligible fraction of the wave function describing the two initial hadrons is absorbed as the collision takes place. The diffraction phenomena to be discussed in this paper are to a large extent simple consequences of the absorption caused by the open inelastic channels. They are characterized by the dimensions of the region of space in which absorption takes place (1 fm). They are, however, more complicated than simple elastic diffraction because hadrons apparently have internal degrees of freedom which may be excited, a strong evidence for their composite nature.

In reviewing this subject we have in mind the non-specialist. Thus we build up our arguments starting in section 2 from elementary considerations on optical diffraction. In section 3 we consider hadron-nucleus collisions. This we find is the best introduction to hadron-hadron phenomenology since nuclei have well defined dimensions. Within the

nucleus the incoming hadron wave is absorbed quite independently of the details of the hadron-nucleon dynamics and the observed scattering depends essentially upon the dimensions of the nucleus. Sections 4 and 5 are then devoted to describing elastic and inelastic hadron-hadron diffraction phenomena. A large sample of experimental data is presented and discussed using both the optical-geometrical point of view developed in sections 3 and 4 (often referred to as the s-channel approach) and a simple form of the phenomenological exchange picture (t-channel approach). The exchange picture of diffraction, with its recent developments and its predictions, is discussed in more detail in the last two sections, where we review some topical questions at ISR and Fermilab energies.

It goes without saying that space does not allow for a complete presentation of this wide subject. We have chosen material which could be fitted into a logical presentation. Complications and further generalization of the optical analogy develop along the way. We hope this will help newcomers to follow, and leave them with some self-contained facts even if their reading does not go until the end. The readers who already know the subject will find in the last sections detailed presentations of recent developments in the interpretation of the phenomena and throughout the paper many figures in which recent data are compiled. In order to be systematic with such complications, we tried whenever possible to stick to a uniform convention to represent data points in the figures which contain data produced at various high energy accelerators: ▼FNAL, □ SLAC, ▽ AGS, ■Serpukhov, ● ISR, ○ PS.

2. DIFFRACTION IN OPTICS AND ITS EXTENSION TO HADRONIC WAVES

2.1 Fresnel-Kirchhoff Theory

Historically the optical analogy has been instrumental in the development of the field reviewed here and many previous presentations have taken it as a starting point (1 - 4). We shall follow a similar track using a language which is suitable to the extension to hadronic physics.

Optics relies on approximations (5). Speaking of diffraction theory one usually refers to the applications of the Huyghens-Fresnel-Kirchhoff approximate method. It can be applied to the propagation of a plane wave of light behind an opaque screen with a "hole" in it (Figure 1) if the wave length λ is much smaller than the dimensions R of the diffracting hole:

$$kR \gg 1 \quad \text{(short wave length condition)}, \qquad 1.$$

where $k = 2\pi/\lambda$. The propagation of a plane light wave being described by means of a complex scalar function $A(x,y,z)$, the basic formula of the theory connects the value A_o of this quantity on a plane Σ, to the value of the same quantity at some point P of the detector plane (5):

$$A(x,y,z) = (k/4\pi i) \int_\Sigma d^2a \; A_o \; S(\vec{a}) \; (1 + \cos\theta') \; \exp(ikd)/d . \qquad 2.$$

The quantity $A_o.S(\vec{a})$ may be interpreted as the amplitude of the wave "just behind" the plane Σ. The quantity $S(\vec{a})$, which corresponds to the S-matrix of scattering theory, describes the variation introduced in the amplitude by the

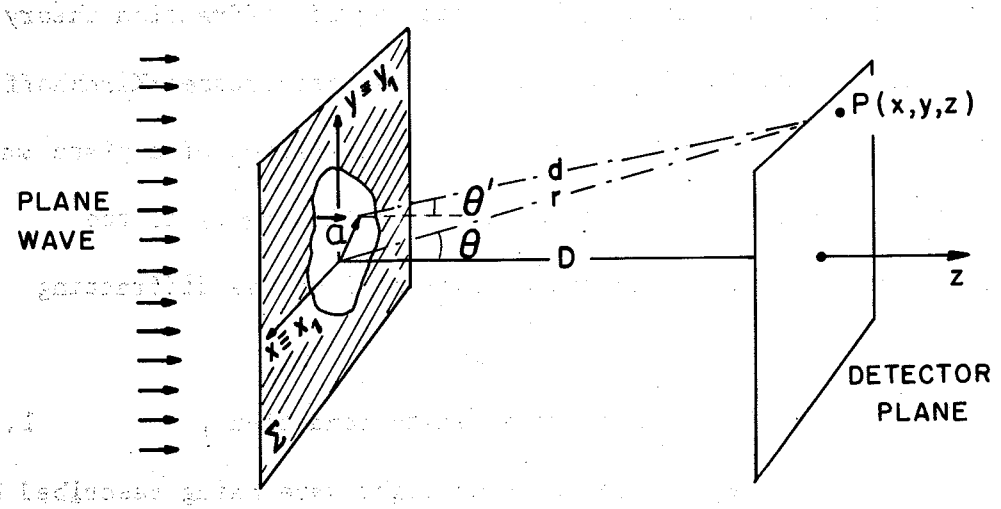

Figure 1 Propagation of a plane wave behind a screen with a hole. Reference systems and definition of the various quantities.

"hole". When the short wave length condition is satisfied, the diffracted wave is concentrated at small angles and the "inclination factor" is practically constant: $(1 + \cos\theta') \approx 2$. The main variation of the factor $\exp(ikd)/d$ comes from the exponent whenever the distance D of the detector plane satisfies the inequality

$$R/D << 1 \quad \text{(large distance condition)}. \qquad 3.$$

The exponent kd may then be written as a power series in the coordinate x_1 and y_1 on the plane Σ and, as is well known, two regimes are distinguished according to the relative values of the quantities $kR >> 1$ and $R/D << 1$:

$$kR^2/D << 1 : \text{Fraunhofer diff.}; \quad kR^2/D \approx 1 : \text{Fresnel diff.} \qquad 4.$$

In the first case the quadratic terms in x_1 and y_1 are negligible and $d \approx r - (xx_1 + yy_1)/r$, while in the second they cannot be neglected. Since geometrical optics is obtained in the limit $\lambda \to 0$, that is $k \to \infty$, for any choice of R and D (i.e. also when condition 3 is not satisfied) one may say that it corresponds to

$$kR^2/D >> 1 \quad \text{(geometrical optics)}. \qquad 5.$$

It is seen that the parameter kR^2/D determines the propagation regime.

Since Fraunhofer diffraction is of great importance for our purpose, it is worth rewriting the diffracted amplitude of equation 2 in this particular case:

$$A(x,y,z) \approx -(ik/2\pi) \left[A_o \exp(ikr)/r\right] \int_\Sigma d^2a \; S(\vec{a}) \; \exp(i\vec{q}.\vec{a}). \qquad 6.$$

The two-dimensional momentum transfer $\vec{q}$ lies in the plane Σ and has by definition components $(kx/r, ky/r)$, so that

$$|\vec{q}| = k\sin\theta. \qquad 7.$$

Let us now consider a diffracting absorbing disc, which is a closer analogy to an absorbing hadron than a screen with a hole. If $S(\vec{a})$ is now the S-matrix for diffraction by the disc, its "profile function" is defined as

$$\Gamma(\vec{a}) = 1 - S(\vec{a}) = 1 - \exp[i\Delta(\vec{a})]. \qquad 8.$$

$\Delta(\vec{a})$ is the complex phase shift. $Im\Delta$ describes the absorption introduced by the disc and $Re\Delta$ is the actual phase shift given to the incoming wave. Introducing $S(\vec{a}) = 1 - \Gamma(\vec{a})$ in equation 6 one obtains the full amplitude behind the disc. The term proportional to 1 is the unperturbed plane wave, and the one which contains $\Gamma(a)$ describes the diffracted wave.

In equation 6 the factor $A_o \exp(ikr/r)$ represents an outgoing spherical wave of amplitude A_o emanating from the centre of the diffracting object to the observation point. The only physically interesting quantity is the factor multiplying this spherical wave, the so-called "scattering amplitude" $f(\vec{q})$. Since $f(\vec{q})$ is proportional to the Fourier transform of the profile function, the converse is also true and one can write:

$$f(\vec{q}) = (ik/2\pi) \int d^2a\, \Gamma(\vec{a}) \exp(i\vec{q}.\vec{a}); \quad \Gamma(\vec{a}) = (1/2\pi ik) \int d^2q f(\vec{q}) \exp(-i\vec{q}\cdot\vec{a}) \qquad 9.$$

When the profile function is spherically symmetric equation 9a simplifies to

$$f(q) = ik \int da\, a\, \Gamma(a)\, J_o(qa). \qquad 10.$$

As much as 140 years ago a similar expression was used by Airy for computing the diffraction of a plane light wave from a circular aperture of radius R. In our notations, he obtained (4)

$$f(q) = ikR^2\, J_1(qR)/(qR). \qquad 11.$$

Equation 10 may be integrated analytically in various cases. Some examples, which will offer a useful guideline later, are presented in Figure 2.

2.2 The Optical Theorem

The optical theorem relates the forward scattering amplitude to the total cross-section σ_t:

$$\sigma_t = 4\pi \, \mathrm{Im} f(0)/k . \qquad 12.$$

For future use we sketch here the derivation of the theorem. The amplitude of the incoming wave is modified by the screen with the factor $S(\vec{a})$, so that the ratio of the energy flux absorbed by the screen to the incident flux is $[1-|S|^2] = 2\mathrm{Re}\Gamma - |\Gamma|^2$. In scattering theory, its integral is the "inelastic cross-section":

$$\sigma_{in} = \int d^2a \, [2\mathrm{Re}\Gamma(\vec{a}) - |\Gamma(\vec{a})|^2] . \qquad 13.$$

Similarly, the differential elastic cross-section $d\sigma/d\Omega$ is defined as the outgoing energy density per unit solid angle normalized to the incoming flux, so that $d\sigma/d\Omega = |f(\vec{q})|^2$. Its integral over the solid angle (with $d\Omega = d^2q/k^2$) gives the "elastic cross-section":

$$\sigma_{el} = \int d^2a \, |\Gamma(\vec{a})|^2 . \qquad 14.$$

The sum of these two quantities is the total cross section σ_t. By comparing it with equation 9a one obtains the optical theorem of equation 12.

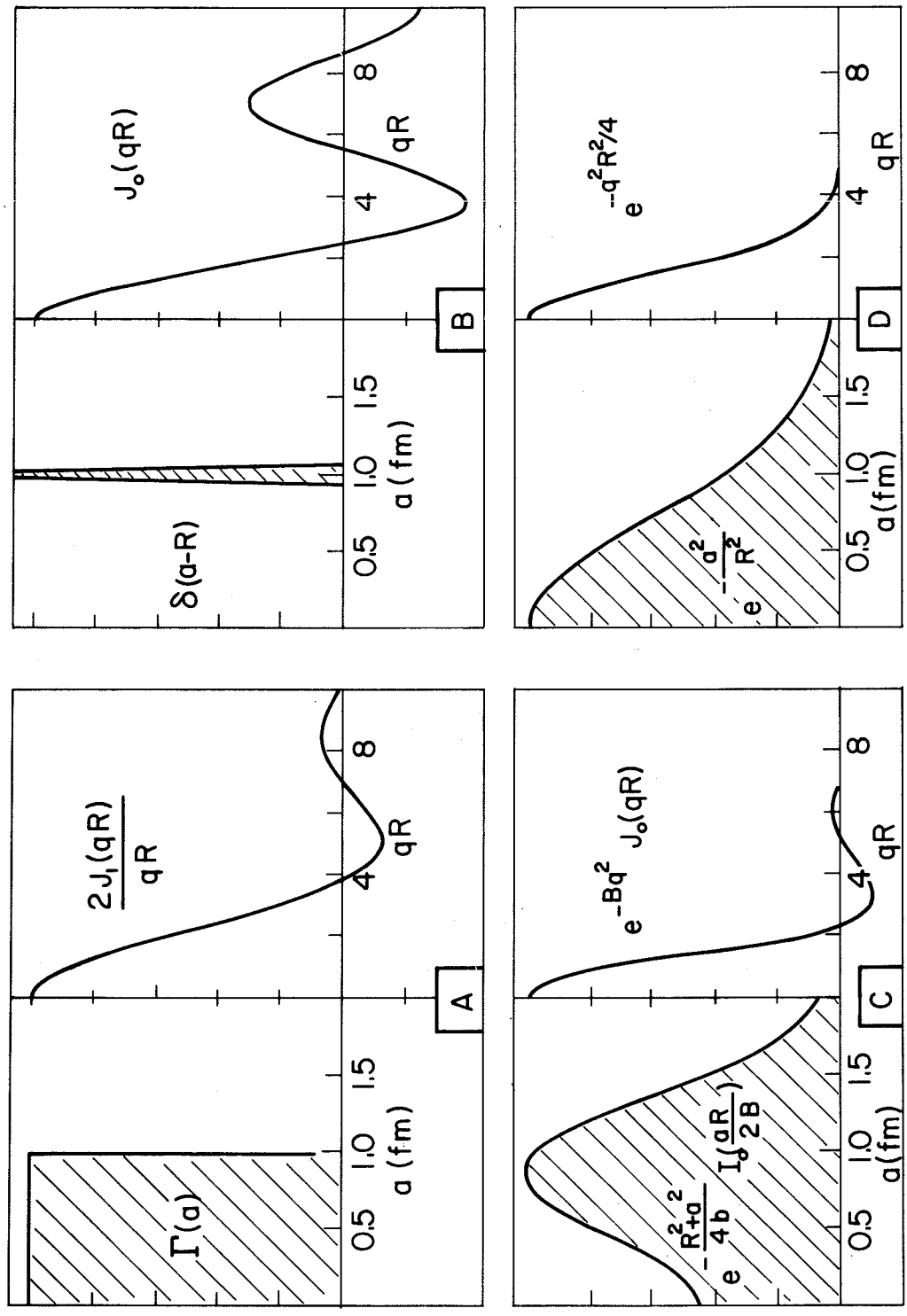

Figure 2 Simple profile functions Γ(a) and the corresponding scattering amplitudes computed by means of eq.10.

2.3 Application of Optical Concepts to Hadronic Waves

Hadrons propagate in free space according to relativistic wave equations where the wave number k is related to the momentum p, the total energy E and the mass m by the usual relation $k = p/\hbar = (E^2-m^2c^4)^{\frac{1}{2}}/\hbar c$. Numerically $k \approx 5.10^{13} p(\text{cm GeV/c})^{-1}$. As pointed out in the Introduction, hadrons as well as nuclei are extended objects. In electron scattering experiments the r.m.s. radii of the charge distributions are actually measured (6). The expression $R \approx 1.1\ A^{1/3}$fm fits the data on nuclei and even gives the reasonable value R = 1.1 fm if for a hadron one takes A = 1. Assuming that hadronic matter has the same distribution as electric charge, the relevant quantity to be introduced in the short wave length condition is kR_t, where k is the wave number in the centre-of-mass system, and R_t is the quadratic combination of the radii of the projectile and the target. For incoming protons to have $kR_t \gtrsim 10$ the laboratory momentum p_L has to be larger than ~ 5, ~ 1 and ~ 0.3 GeV/c when the targets are protons, ^{4}He nuclei and ^{208}Pb respectively. The same limits are applicable, within 20%, if the incoming hadrons are pions instead of protons.

The large distance condition 3 is always satisfied because the distance D at which the scattered hadrons are observed behind the scatterer is at least of the order of 1 cm, so that $R/D \simeq 10^{-13}$. Since in all experiments performed so far kR is never larger than 10^4, the quantity kR^2/D is always smaller than 10^{-9}. Therefore hadron-hadron and hadron-nucleus scattering is analogous to Fraunhofer diffraction.

Typical diffraction patterns appear in the differential cross-sections of Figure 3. As a first application of optical concepts we

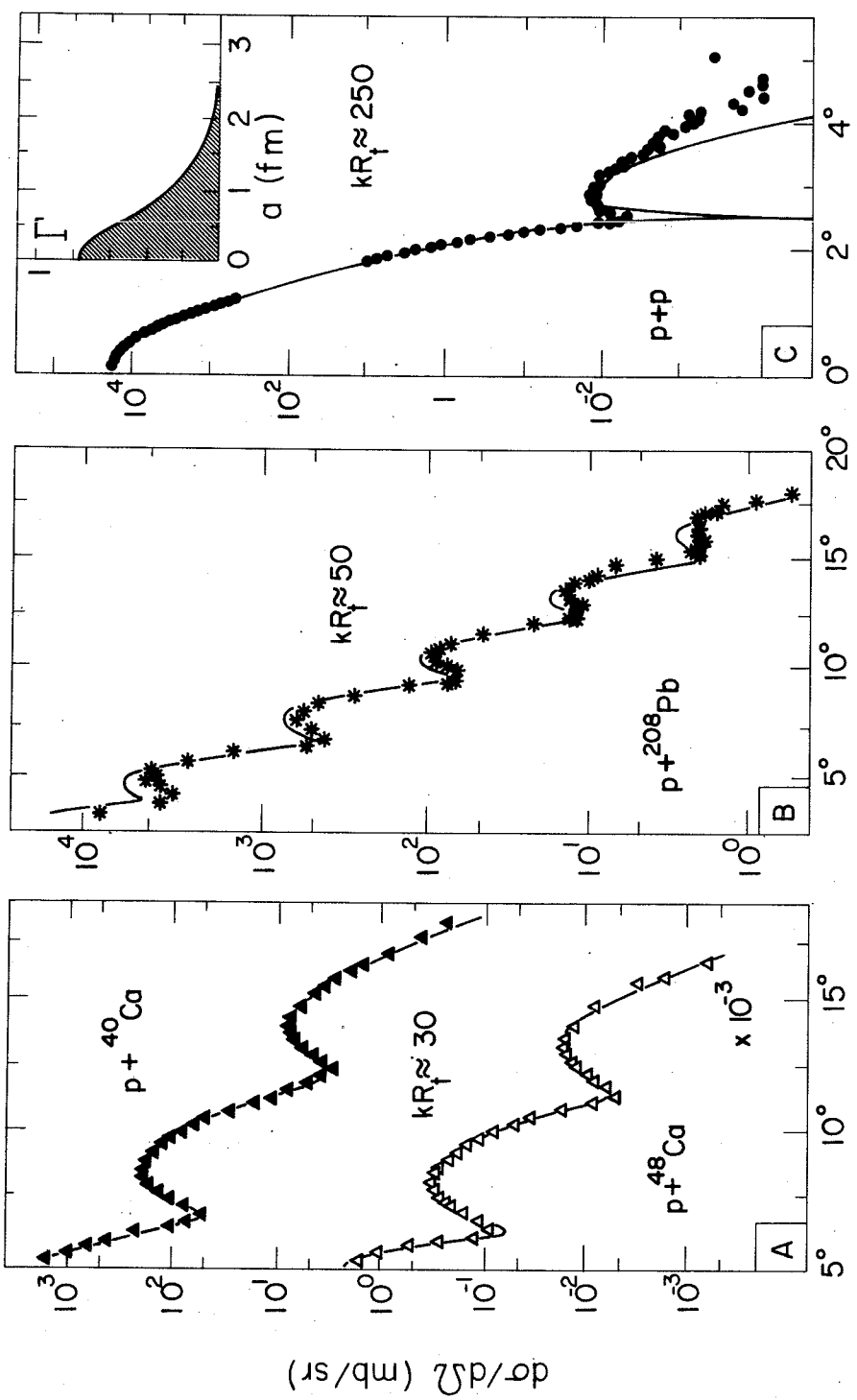

Figure 3 Typical diffraction patterns produced by hadronic waves: (A) elastic scattering of protons of 1.7 GeV/c on ^{40}Ca and ^{48}Ca (7). The fits are based on Glauber theory. (B) Elastic scattering of protons of 1.75 GeV/c on ^{208}Pb (8). The curve is computed applying Glauber theory (10). (C) Elastic scattering measured at the CERN Intersecting Storage Rings (ISR) by the Aachen-CERN-Genova-Harvard-Torino Collaboration (11a). The equivalent laboratory momentum of the proton is p_L = 1480 GeV/c. The curve is a fit (11b) based on the optical model of Chou and Yang (33-35).

may consider the calculation of the profile functions. This already meets with a problem, since the complex scattering amplitude is needed in equation 9b, while the differential cross-section gives only information on its modulus: $|f| = \sqrt{d\sigma/d\Omega}$. The phase of the amplitude at $\vec{q} = 0$ may be obtained by measuring the interference between the nuclear and the Coulomb amplitude. In subsection 4.4 it will be shown that the amplitude $f(0)$ is essentially imaginary, i.e. that its phase is close to 90^{o} in hadron-hadron collisions, at least for laboratory momenta larger than 10 GeV/c. For $\vec{q} \neq 0$ the phase of the nuclear scattering amplitude must be derived from some model. The simplest one corresponds to a purely absorbing interaction, i.e. to an imaginary phase-shift $\Delta(\vec{a})$ and a real $\Gamma(\vec{a})$. This is an over-simplification. Nevertheless the fact that it is a reasonable one at very high energies justifies the present interest in optical diffractive models. In this case the amplitude of equation 10 is imaginary at all momentum transfers and one speaks of "shadow scattering". This model is applicable when the energy is large enough and thus there are many open inelastic channels summing up to a large inelastic cross-section ($\Gamma(0)$ real and not too far from 1 in equation 13). In such circumstances the elastic scattering is mainly the shadow of the inelastic channels and the momentum transfer dependence reflects the shape of the interacting hadrons. The profile function plotted in the inset of Figure 3C has been obtained within this model. This brings a question and a remark.

Question. What is the meaning of the parameter $\vec{a}$ in the case of hadron-hadron collisions? This may be clarified by writing the incoming hadron wave as a sum of partial waves of orbital angular momentum ℓ and

then by approximating the sum over ℓ by an integral over the variable $a \simeq (\ell + 1/2)/k$. If the energy is large enough so that a very large number of partial waves contributes, the wave length is so small that a semi-classical description of the scattering process is applicable (4). The quantity $\vec{a}$ is nothing else but the minimum distance of approach between the centres of the two colliding hadrons. For this reason it deserves the name of "impact parameter". Since the range R of the hadron-hadron forces is finite, their effect drops exponentially at large distances and the relevant angular momenta may increase in number as $\ell_{max} \lesssim kR\ell n(kR)$. (We would have kR for a sharp edge). The short wave length condition becomes $\ell_{max} >> 1$: the diffraction picture applies in its simplest form when many partial waves contribute. They are almost purely imaginary and coherence effects are maxima.

Remark. Experimentally it is found that the hadron-hadron differential cross-section close to the forward direction is a gaussian in the scattering angle (Figure 3C). Thus the scattering amplitude is well represented by the form

$$f(q) = k\sigma_t(i+\rho)\ \exp(-b|t|/2)/4\pi \qquad 15.$$

where the ratio ρ between the real and the imaginary part is taken to be energy independent. The parameter b is the "slope" of the logarithm of the differential cross-section plotted versus $|t| = \hbar^2 q^2$. [1] The profile function corresponding to equation 15 is gaussian and Figure 2D shows

1 The four-momentum transfer squared t is given by $t=2\ m^2c^4-2(E_1E_2-p_1p_2c^2\cos\theta)$ where $(E_1,\vec{p}_1)$ and $(E_2,\vec{p}_2)$ are energies and momenta of the scattered hadron, with mass m before and after the collision.

that its radius is

$$R = \hbar 2^{\frac{1}{2}} b^{\frac{1}{2}} \approx 0.3\ b^{\frac{1}{2}} \text{fm} \quad (b \text{ in GeV/c}). \qquad 16.$$

For $R \approx 1$ fm this relation gives $b \approx 10\ (\text{GeV/c})^{-2}$.

2.4 Polarization Effects in Optics and Diffraction Dissociation

Our discussion has so far been limited to a scalar amplitude. It is, however, well known that when polarization is considered, new phenomena appear in optical diffraction. Let us for instance consider a screen with a "hole" which has different indices of refraction for right and left circularly polarized beams (a tube with a sugar solution in it). In this case there are two profile functions $\Gamma_R(\vec{a})$ and $\Gamma_L(\vec{a})$ which form a two-by-two diagonal matrix in the representation which uses right and left circularly polarized states as base vectors. In a linear polarization basis the profile matrix is no more diagonal, so that the diffraction of a linearly polarized beam gives rise to <u>two</u> different waves. The first has the same polarization as the incident one and scattering amplitude proportional to the Fourier transform of $(\Gamma_L + \Gamma_R)$, while the second is polarized at 90^o and is determined by the profile function $(\Gamma_L - \Gamma_R)$. This second component is not present in the incident wave and may be regarded as the production by diffraction of a new state degenerate in energy (frequency) with the initial state. We note that such a diffractive production becomes possible since a new degree of freedom is introduced in the description of the incoming wave.

About twenty years ago Glauber (12), Feinberg and Pomeranchuk (13), Good and Walker (14) and others pointed out that similar effects must exist in the interaction of hadrons with nuclei. In the Good and Walker approach, one views

the state $|i\rangle$ of a hadron h_0 which moves through a nucleus as a linear combination of states $|n\rangle$ which have the same intrinsic quantum numbers as the hadron and are eigenstates for strong interactions in nuclear matter: $|i\rangle = \Sigma C_{ni} |n\rangle$. The S-matrix is diagonal in the space spanned by the diffractive eigenstates $|n\rangle$ and "just behind" the nucleus the wave has the form $S(\vec{a})|i\rangle = \Sigma C_{ni} [1 - \Gamma_n(\vec{a})]|n\rangle$. In general the profile functions Γ_n of the various states $|n\rangle$ are not all equal so that the diffracted wave does not coincide with the initial physical hadron. Let $\Gamma(\vec{a})$ be the profile function describing diffraction scattering of h_0. The leftover diffracted wave just behind the nucleus is then $\Sigma C_{ni} [\Gamma(\vec{a}) - \Gamma_n(\vec{a})]$, which expresses the fact that each state $|n\rangle$ is present with an amplitude which is proportional to the difference between the profile function for elastic scattering of the hadron h_0 and the profile function referring to the eigenstate $|n\rangle$. Diffraction dissociation is thus expected to be small where these differences are small, for instance at the centre of a heavy nucleus which is completely absorbing for most states $|n\rangle$. This already indicates that diffraction dissociation is expected to be more peripheral, in impact parameter space, than elastic shadow scattering.

The physical states $|f\rangle$ that are observed far away from the nucleus are linear combinations of the eigenstates $|n\rangle$ and in general do not appear as single particle states but rather as systems of two or more hadrons with energy M in their centre-of-mass and of global laboratory momentum P. Nuclear coherence puts restriction on the possible systems h which may be diffractively produced. Indeed they must have the same intrinsic quantum numbers of the incoming hadron h_0, i.e. the same charge, isotopic spin, nucleon number, strangeness, charge conjugation etc. However, they

need not keep the spin and parity of h_0, because some angular momentum may be transferred to the internal motion of the hadron while the total angular momentum stays constant. A further limitation comes from the request of coherent production: the mass M should not be too different from the mass m of the incoming hadron. For zero angle production the momentum transfer is $(p-P) \approx (M^2-m^2)c^2/2p$, so that for a given incoming momentum p the minimum four-momentum transfer at which the mass M may be produced is

$$t_{min} = \left[(M^2-m^2)c^2/2p\right]^2 . \qquad 17.$$

In the transition the wave number k of the incident hadron varies by $\Delta k = (p-P)h$. The condition of coherent production amounts to the request that the product of Δk by the radius R of the diffracting nucleus has to be smaller than 1. Only in this case can the waves describing the hadron h_0 and h stay in phase within the nucleus. In summary we have [2]

$$\text{coherence condition:} \quad M^2-m^2 \lesssim 2p/R. \qquad 18.$$

Good and Walker's idea applies not only to hadron-nucleus, but also to hadron-hadron collisions. In this case the basis $|n\rangle$ is defined as the set of states which do not mix in the interaction. The coherence condition is easier to satisfy since the radius R is smaller.

Evidence for diffraction dissociation of negative pions is shown in Figure 4. The data were collected at the CERN PS by the CERN-Milan-ETH (Zürich)-Imperial College collaboration (15-20) on the reaction $\pi^- + A \to (\pi^-\pi^+\pi^-) + A$ around 15 GeV/c of laboratory momentum. It is seen that the mass distributions of the produced three pion system peaks at low masses and that masses around 1.7 GeV are relatively more abundant

[2] From now on we shall put $\hbar = c = 1$, so that energy, mass and momentum transfer are all measured in GeV.

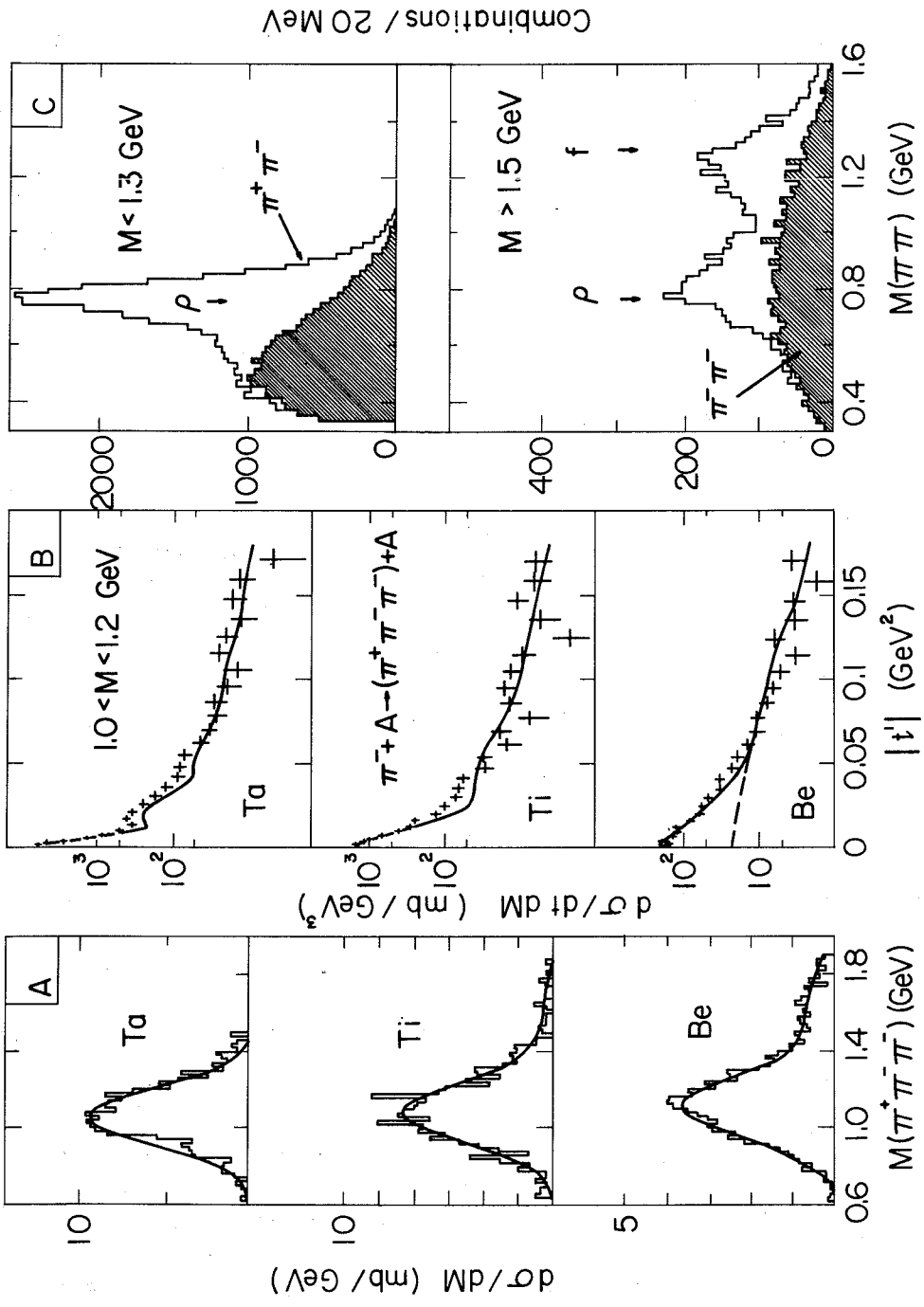

Figure 4 Diffraction dissociation of 15 GeV/c π^- on nuclei (15-20):

(A) Mass distributions of the 3π system on tantalium, titanium and berillium nuclei.

(B) Differential cross section on the same three targets as a function of $t' = t - t_{min}$. The curves are fits based on Glauber theory (51).

(C) Two-pion spectra for two samples of data having different 3π masses.

with a berillium target than with a tantalium one. This agrees with the coherence condition which is better satisfied for smaller nuclei. Moreover the angular distributions show a very pronounced forward peak whose slope b increases as $A^{2/3}$, i.e. as R^2 as predicted by equation 16. These data will be discussed in more detail in section 3.3

3. DIFFRACTION IN HADRON-NUCLEUS COLLISIONS

We now consider hadron-nucleus scattering as a second step towards the identification of the general properties of diffraction phenomena in hadron-hadron collisions. Heavy nuclei are a useful tool because they have a well defined radius R, which may be varied by changing the mass number, and because hadrons are much absorbed for impact parameters smaller than R. Moreover a reliable theory exists to describe diffraction in hadron-nucleus scattering and what happens depends more on the size of the nucleus than on the details of the interaction with each nucleon. In the following we shall sketch the main lines of Glauber theory (21-24) not only to discuss elastic hadron-nucleus collisions but also to prepare the presentation of some geometrical models of hadron-hadron scattering.

3.1 Diffraction Theory of Coherent Hadron-Nucleus Scattering

Glauber theory describes the scattering of a hadronic wave by a system composed of various scattering centres. It is applicable to small momentum transfer scattering. It is based on three main hypotheses: (A) the nuclear wave function has no time to change during the propagation of the hadron inside the nucleus; (B) the propagation of the hadronic wave within the nucleus follows the laws of geometrical optics; (C) the

phase shifts produced by the individual nucleons combine additively. We briefly consider the rationale for these hypotheses.

The first hypothesis is satisfied for laboratory momenta of the incident hadron larger than $\sim$ 1 GeV/c, i.e. whenever the incident energy is much larger than the excitation energies of the nucleus (25).

According to the discussion of subsection 2.1, the second condition is satisfied when $kR^2 >> D$, where R is the interaction radius in a hadron-nucleon collision and D is the radius of the nucleus. This condition is also satisfied for $p_L \gtrsim$ 1 GeV/c. (Gottfried has shown that some Fresnel effects are present in hadron-deuteron scattering below 1 GeV/c (26)).

Condition (C) does not represent a further assumption if the hadron-nucleon interaction can be described by a local potential (4), since the phase shift depends linearly on the potential and the potentials due to the different nucleons sum up. However, at high enough energies the phases $\Delta_j(a)$ due to the interaction of the j-th nucleon with the incoming hadron are complex and condition (iii) becomes an independent hypothesis.

The S-matrix for the hadron-nucleus interaction takes the form

$$S_A(\vec{a};\vec{s}_1 \ldots \vec{s}_A) = \prod_{j=1}^{A} \exp\left[i\Delta_j(\vec{a}-\vec{s}_j)\right], \qquad 19.$$

where $\vec{s}_j$ is the transverse position of the j-th nucleon (Figure 5). The nucleus profile function can then be written as the sum of A terms

$$\Gamma_A(\vec{a};\vec{s}_1 \ldots \vec{s}_A) = \sum_i \Gamma_i(\vec{a}-\vec{s}_i) - \sum_{i>j} \Gamma_i(\vec{a}-\vec{s}_i)\Gamma_j(\vec{a}-\vec{s}_j) + \qquad 20.$$

$$\sum_{\substack{i>j>k}} \Gamma_i(\vec{a}-\vec{s}_i)\Gamma_j(\vec{a}-\vec{s}_j)\Gamma_k(\vec{a}-\vec{s}_k) - \ldots .$$

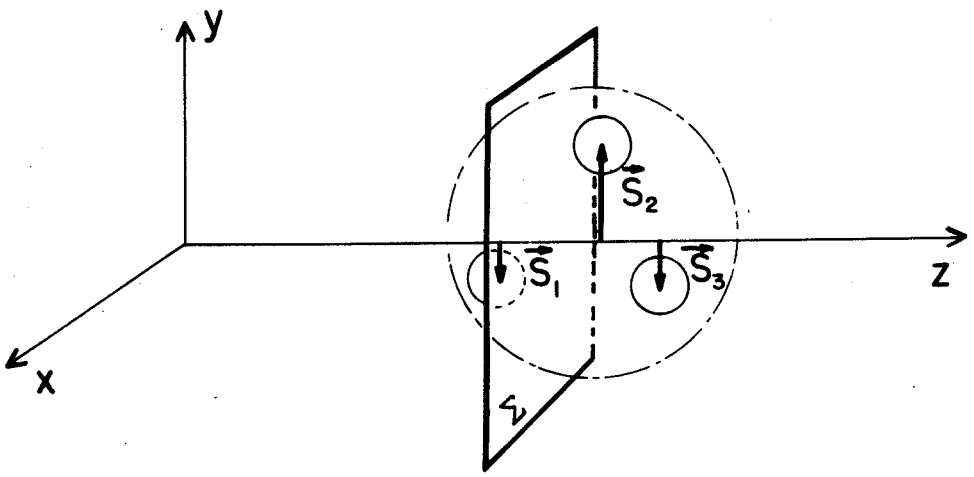

Figure 5 Definition of transverse positions in the Glauber approach.

This equation expresses the nucleus profile function in terms of the nucleon profiles and shows that, when the interaction is weak ($\Gamma_i \approx 0$), the profile functions of such a "frozen" nucleus is equal to the sum of the profile functions of its constituent nucleons. This is not the case in general, however, and the other terms of this "multiple scattering series" have also to be taken into account. For instance, the second term represents events in which the incoming hadron is scattered by two different nucleons in the nucleus, the third term represents triple scattering and so on.

3.2 Elastic Scattering of Hadrons on Nuclei

For light nuclei the number of terms in the Glauber multiple expansion is small and may be computed explicitely by introducing a suitable parametrization of the hadron-nucleon profile. (A gaussian profile is usually used, as implied by equation 15.) In Figure 6 experimental data on pion-deuteron scattering (27-29) are compared with such a calculation (29-31).[3] The forward peak is associated with the first term in the expansion. It represents single scattering of the pion either from the proton or from the neutron in the deuteron acting coherently. Its momentum transfer dependence is essentially that of the deuteron form factor. For $|t| \gtrsim 0.5$ GeV^2, however, the second (and last) term in equation 20 dominates: this corresponds to double scattering when the pion hits succes-

[3] Proton-nucleus data have been reviewed by Saudinos and Wilkin (24a) and by Ciofi degli Atti (24b).

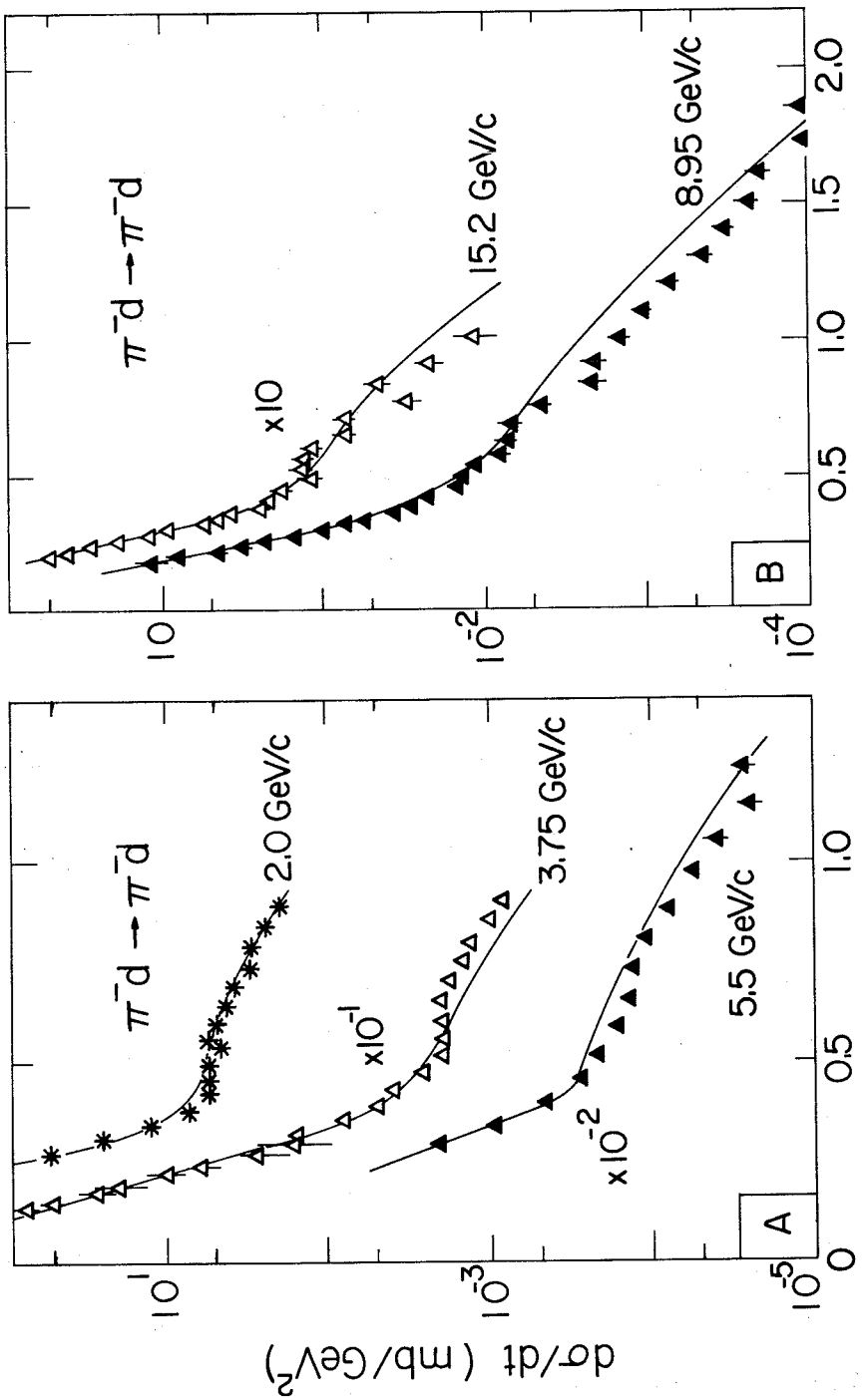

Figure 6 Data on pion-deuteron elastic scattering at different momenta (27-29) are compared with calculations based on Glauber theory (30).

sively the neutron and the proton. It requires more localization in space and hence the t-dependence is less sharp than in the former case.

For intermediate and heavy nuclei the profile operator of equation 20 contains many terms. The previous method becomes cumbersome and a simpler and yet reliable description of hadron-nucleus elastic scattering is obtained neglecting correlations in the nuclear wave function, so that the ground state can be described by the nuclear densities $\rho_j(\vec{r})$ of the A nucleons ($\int d^3r\ \rho_j(\vec{r}) = 1$). Then the expectation value of the S-matrix in the nucleus ground state $|0>$ takes the form

$$<0|S_A(\vec{a})|0> = \prod_{j=1}^{A} \int d^2s\ dz\ \rho_j(\vec{s},z)\ [1-\Gamma(\vec{a}-\vec{s})]\ , \qquad 21.$$

where $\Gamma(\vec{a})$ is the hadron-nucleon profile. For $A \to \infty$ the product of these A factors may be written in the form $\exp(i\Delta_A)$ where

$$i\Delta_A(\vec{a}) = -\int d^2s\ \Gamma(\vec{a}-\vec{s}) \int_{-\infty}^{+\infty} dz\ \rho(\vec{s},z) = -\int d^2s\ \Gamma(\vec{a}-\vec{s})\ T(\vec{s}) \qquad 22.$$

In this equation $\rho = \Sigma\rho_j$ is the total nuclear density ($\int d^3r\rho = A$) and $T(\vec{s})$ is the "thickness function", i.e. the integral of the density along a straight path at impact parameter $\vec{s}$. Equations 21 and 22 are the starting point for most calculations of elastic scattering of high energy hadrons on intermediate and heavy nuclei. For instance, the curves in figure 3A have been computed with equation 21 (7). The nuclear matter distribution needed to fit the ^{40}Ca data comes out to be very similar to the charge distribution measured in electron-nucleus scattering. Similarly, the curve of figure 3B is computed without adjustable paramters, using a self-consistent density distribution derived from Hartree-Fock calculations (10). In summary the theory of

hadron-nucleus diffraction is precise enough to provide information on the nuclear density of accuracy comparable to the one derived from electron scattering. This conclusion was already reached a few years ago (32).

To understand how the apparently smooth expression 22 gives rise to the many oscillations appearing in the differential cross-section, it is useful to introduce the Fourier transform of the phase

$$\Delta_A(\vec{q}) = (1/2\pi) \int d^2a \exp(i\vec{q}.\vec{a})\ \Delta_A(\vec{a}) = A\ f(\vec{q})\ F(\vec{q})/(ik) \qquad 23.$$

$f(\vec{q})$ is the hadron-nucleon scattering amplitude and $F(\vec{q})$ is the form factor of the nucleus so normalized that $F(0) = 1$. The hadron-nucleus scattering amplitude $f_A(\vec{q})$ is the Fourier transform of $\{1 - \exp[i\Delta_A(\vec{a})]\}$ and, expanding this exponential, it may be formally written as a series in $\Delta_A(\vec{q})$, namely

$$f_A(\vec{q}) = ik(\Delta_A(\vec{q}) - \Delta_A(\vec{q}) \otimes \Delta_A(\vec{q})/2! + \Delta_A(\vec{q}) \otimes \Delta_A(\vec{q}) \otimes \Delta_A(\vec{q})/3! \ldots). \qquad 24.$$

The convolution of two functions in momentum space is defined as

$$N(\vec{q}) \otimes M(\vec{q}) = (1/2\pi) \int d^2q'\ N(\vec{q})\ M(\vec{q}-q'). \qquad 25.$$

If the interaction of the hadron with the nucleons is not very strong, the first term is sufficient, and the differential cross-section is simply

$$(d\sigma/d\Omega)_{coher} = A^2\ |f(q)|^2\ F^2(q)\ , \qquad 26.$$

It has the typical A^2 dependence of a coherent process. The q-dependence of this expression is mainly determined by the nuclear form factor, i.e. by the size of the nucleus. The other terms in the expansion alternate in sign and give rise to the typical oscillatory behaviour superimposed on the rapid decrease determined by the form factor. Note that if $\Delta_A(q)$ is approximated by $\exp(-cq^2)$, the n-term of the development is

proportional to $\exp(-cq^2/n)$, so that each successive term gives a flatter contribution which eventually dominates at larger angles.

An extension of equation 22 has been used by Chou and Yang to interpret elastic scattering in very high energy proton-proton collisions (33-36). This approach is based on the idea that hadrons are extended distributions of nuclear matter made up of an infinite number of very small constituents. The constituents of the two hadrons interact locally, i.e. their profile is a delta function. The phase $\Delta(\vec{a})$ of this model is immediately written down as an extension of equation 22, which was obtained for a hadron interacting with a nucleus having thickness function $T(\vec{s})$. If T_A and T_B are the thickness functions of the interacting hadrons, the Chou and Yang phase is proportional to the integral $\int d^2s\ T_A(\vec{a}-\vec{s})T_B(\vec{s})$. The thickness function is then obtained from the charge distribution, i.e. from the measured electromagnetic form factors F_A and F_B of the two hadrons. With this hypothesis the Fourier transform of the phase, defined by equation 23, becomes $\Delta(q) = C_{AB}F_A(q)F_B(q)$. C_{AB} measures the strength of the interaction and is the only free parameter of the model. In the case of proton-proton scattering the first term of the development 24 gives a cross-section proportional to $F_p(q)$. The interference with the second term, negative and less steep, gives rise to a minimum at t 1.5 GeV . The curve of Figure 3C is the result of such a calculation (11b). The data are very well reproduced. It must be stressed that the model was suggested to be valid at infinite energy, when a limiting angular distribution was supposed to be reached. As it will be discussed, the results of the CERN Intersecting Storage Rings have shown that up to 2000 GeV/c no limiting distribution is

reached. One must conclude that the Chou-Yang approach is too simple, yet it has many appealing features.

3.3 Exclusive Diffraction Dissociation of Hadrons on Nuclei

Pion diffraction dissociation is illustrated in Figure 4, which contains a sample of the data of the CERN-Milan-ETH-Imperial College collaboration. More data may be found in Lubatti's review article (37), where results on nuclear targets are presented in parallel with data on nucleons. Figure 4B shows that the slope of the forward cross-section increases proportionally to the square of the nuclear radius.
The mass spectrum of the three pion system peaks around M = 1.1 GeV and, for light nuclei, it shows another structure at M $\approx$ 1.7 GeV (Figure 3A). These bumps are associated with the names of "A_1 and A_3 enhancements". The study of their properties has been one of the main issues in the field of exclusive diffraction dissociation in the past few years. Some properties of these systems are illustrated in figure 4C, where, from the data of the same collaboration, summed over all targets, mass spectra for pairs of pions have been constructed. While the combination $\pi^-\pi^-$ has a structureless behaviour, the peaks present in the $\pi^+\pi^-$ combination show that the three-pion system of mass smaller than 1.3 GeV/c^2 decays predominantly via the channel $\rho^0(780) + \pi^-$, while for masses larger than 1.5 GeV one finds both $\rho + \pi^-$ and $f(1270) + \pi^-$ configurations.

Refined partial wave analysis of the three pion system diffractively produced on hydrogen targets have been performed by the Illinois group (38) and will be discussed in subsection 5.2. The same analysis was used both in the experiment under discussion and in a more recent one performed at 23 GeV/c at the Brookhaven AGS by the Carnegie Mellon-Northwestern-

Rochester collaboration (39-41). In these experiments coherent production on nuclei was shown to be dominated by states in which the three pions have total angular momentum and parity $J^P = 0^-$ and 1^+ in the region of the A_1 and 2^- in the region of the A_3. Here we meet for the first time with a regularity which we shall encounter again in the following discussion: the pion, which has $J^P = 0^-$, diffractively dissociates in states which belong to the J^P series 0^-, 1^+, 2^- (unnatural parity states).

Kaon diffraction dissociation on nuclei has been studied first in heavy liquid bubble chambers and later with counters by the CERN-Milan-ETH-Imperial College collaboration (17). The ($K\pi\pi$) mass spectrum, which presents similarities to the 3π spectrum, shows a prominent bump at $M(K\pi\pi) \approx 1.3$ GeV, referred to as the Q-enhancement. At larger masses (~ 1.75 GeV) a small structure appears, usually named L-enhancement, which is again not visible in heavy nuclei. This is due to the coherent condition. The Q-enhancement has a strong contribution of 1^+ nature and decays mainly through the channel $K^*(890)\pi$ and ρK, thus paralleling the behaviour of the A_1, which decays into $\rho\pi$. Again we see that a 0^- particle dissociates preferentially in a 1^+ state.

Nucleon diffraction dissociation experiments have been recently performed at the Brookhaven AGS. The Michigan group has studied the reaction $n + A \rightarrow (p\pi^-) + A$ (42) and the Carnegie Mellon-Northwestern-Rochester collaboration has collected high statistics data at $p_L = 22.5$ GeV/c on the reaction $p + A \rightarrow (p\pi^+\pi^-) + A$ (40, 43). The angular distributions measured on C, Cu and Pb are plotted in Figure 7 versus $t' = t - t_{min}$ together with the mass spectra of the $(p\pi^+\pi^-)$ system. In this case too, there is a prominent bump at $M \approx 1.4$ GeV and, for carbon target, a small enhancement

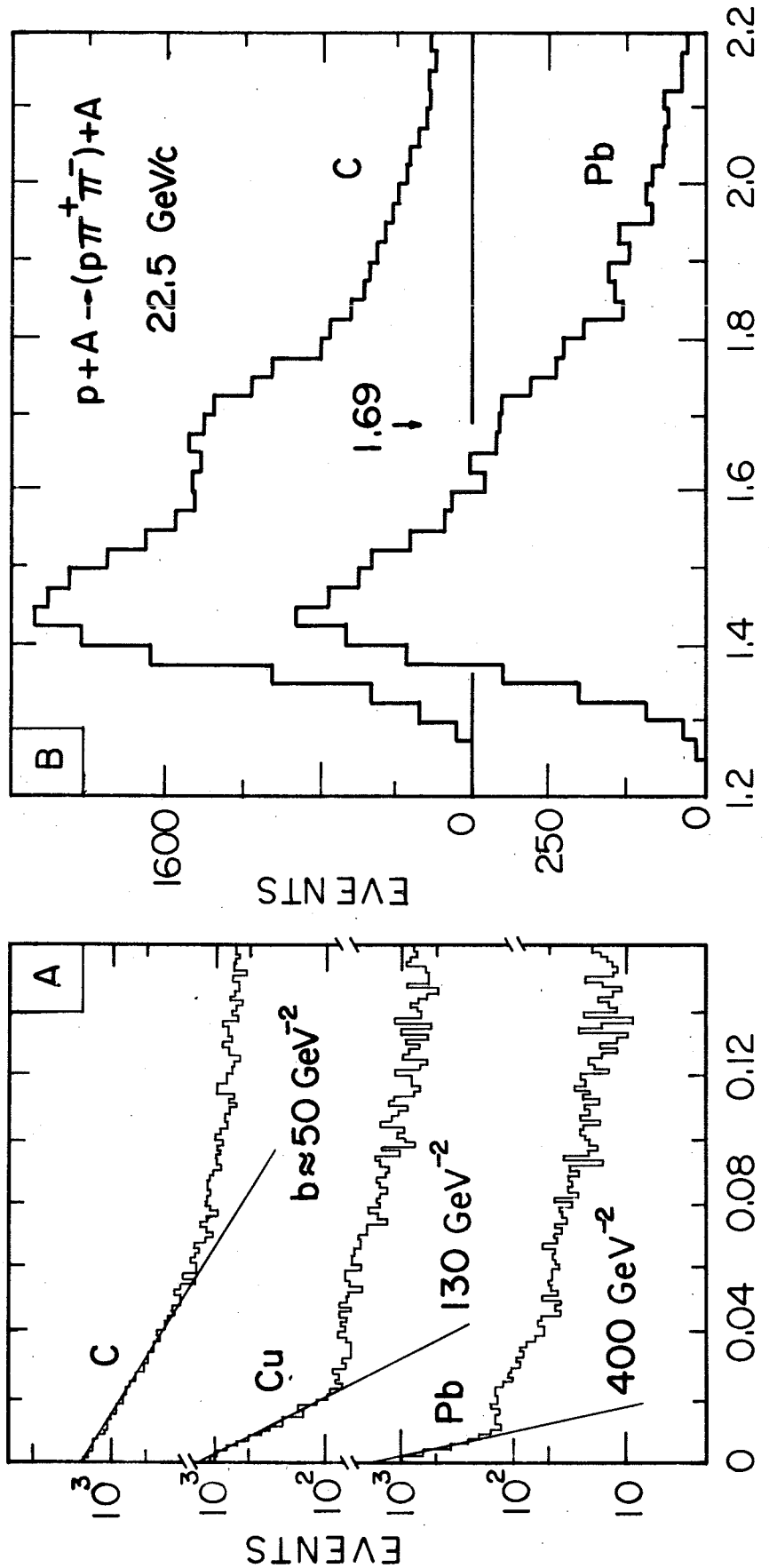

Figure 7 Proton diffraction dissociation on nuclei measured by the Carnegie Mellon-Northwestern-Rochester Collaboration.
(A) The forward peak has a shape which is roughly proportional to the square of the nucleus radius. This is a clear indication of the diffractive nature of the process.
(B) Mass spectra of the $(p\pi^+\pi^-)$ produced on carbon and lead targets.

around 1.7 GeV. The first is a typical threshold enhancement of spin-parity $1/2^+$. (It compares to what was found with the A_1 and Q). The second is very probably due to coherent production of the $5/2^+$ state N(1690). Thus for half integer projectile diffraction dissociation favours transition of the type $1/2^+ \rightarrow 1/2^+$, $1/2^+ \rightarrow 5/2^+$.

Proton diffraction dissociation on deuterons has been recently studied in a very elegant experiment by the Fermilab-Dubna-Rockefeller-Rochester collaboration working on the circulating proton beam of the 400 GeV/c Fermilab synchrotron (44, 45). The technique, using a gas jet of hydrogen (or deuterium) as a target for protons circulating in the machine during the acceleration cycle, has been discussed in detail by Melissinos and Olsen (46). By measuring the kinetic energy and the angle of the proton (or deuteron), which for small momentum transfers t recoils at an angle close to 90^0, one can determine both the value of t and the mass M of the produced system. Momentum transfer distributions obtained at p_L = 275 GeV/c for three values of M are plotted in Figure 8A. The steep fall-off is mainly determined by the deuteron form factor and is due to the fact that at very small momentum transfer the double scattering contribution is negligible. In analogy with equation 26, the differential cross-section for diffraction dissociation factorizes, namely

$$(d^2\sigma/dtdM)_{pd} = (\sigma_t^{pd}/\sigma_t^{pp})\ F^2(t)\ d^2\sigma/dtdM, \qquad 27.$$

where F(t) is the deuteron form factor. The ratio of the cross-section is $\sim$ 3.6, and substitutes in equation 26 the factor $A^2 = 4$, so as to take into account shadowing effects. Equation 27 is used to extract proton - nucleon cross-sections from proton- deuteron data.

Proton-proton missing mass spectra derived from proton-deuteron data at p_L = 50 and 275 GeV/c are compared in Figure 8B with previous proton-proton data at 20 GeV/c obtained at the AGS (47). The broad bump at $M^2 \approx 2$ GeV^2 is attributed to the production of the 1.4 GeV "enhancement" and the structure at 1.7 GeV is identified with the excitation of the well-known resonant state N(1690).

In the above examples diffraction dissociation is identified by the presence of a large forward peak the slope of which is related to the dimension of the nucleus. This small sample of data agrees with what is also found in hadron-hadron dissociation: not all energetically possible states are diffractively produced.Not only the intrinsic quantum numbers are preserved in the process, but also the Gribov-Morrison empirical rule seems to hold quite generally (48,49). This rule is expressed by

$$P_f = P_i \, (-1)^{\Delta J} \; ; \qquad 28.$$

P_i and P_f represent the parity of the initial and final systems and ΔJ is the change of spin. In words, the change of parity is that which corresponds to the net gain in spin. This in turn corresponds to the minimum transfer of orbital angular momentum. For diffraction dissociation of the pseudoscalar mesons (π and K), the Gribov-Morrison rule allows the production of states with unnatural parity 0^-, 1^+, 2^-, 3^+ etc., while for diffraction dissociation of nucleons the allowed sequence is $1/2^+$, $3/2^-$, $5/2^+$, $7/2^-$ etc. For the collision of spinless particles at t = 0 this rule is equivalent to the conservation laws of parity and angular momentum (48). Goldhaber and Goldhaber have shown that, to order A^{-1}, the same behaviour is predicted for spinless hadrons diffracting on nuclei of non-zero spin (50). Away from the forward direction the rule implies some selective

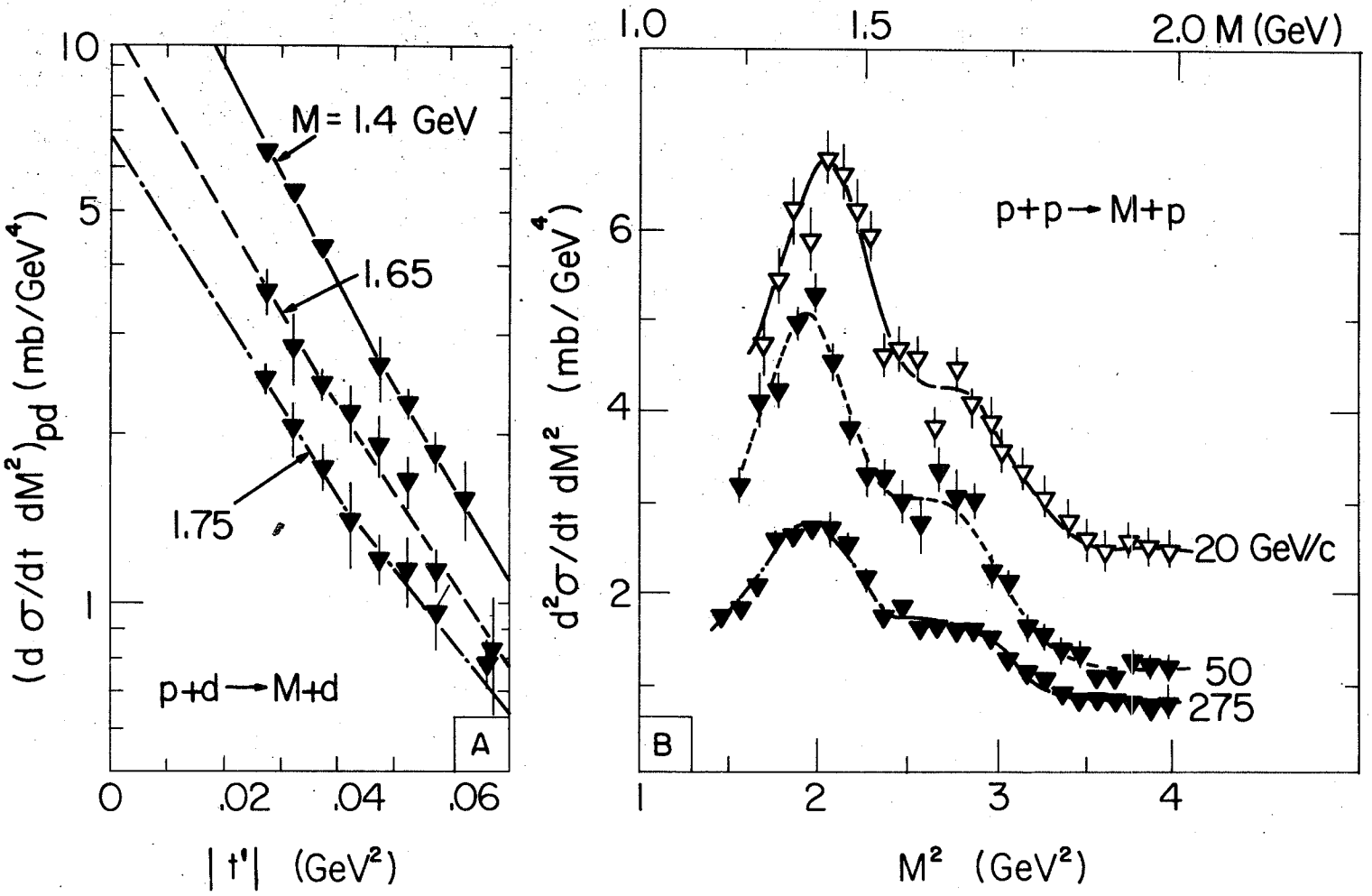

Figure 8 Proton diffraction dissociation on deuterons at small momentum transfers (44-46).

(A) Differential cross sections plotted versus $t' = t - t_{min}$ for various masses M of the produced system.

(B) The black triangles represent the mass spectra in the reaction p + p → M + p measured at 50 and 275 GeV/c for $|t| \approx 0.04$ GeV^2. They were obtained by the USSR-USA Collaboration working at Fermilab from the deuteron data by means of eq. 27. The open triangles were measured at the AGS (47). The curves are only to guide the eye.

dynamical mechanism. The rule may often be enforced since, as the momentum transfer increases, the cross-section is damped by the usual factor, which for coherent production on nuclei is proportional to $F^2(q)$ (equation 26). As a consequence a production amplitude, which is zero in the forward direction, will never have a chance to become appreciably large. However, this argument cannot be used to justify a rigorous rule. Thus equation 28 has to be considered an empirical relation whose dynamical origin has still to be understood. Indeed some recent data even contradict it. For instance the pion-dissociation experiment of the Carnegie Mellon-Northwestern-Rochester collaboration on C, Al, Cu and Ag targets indicates that the rule is not satisfied, since in the partial-wave analysis of the data (41), evidence is found for coherent production of the $A_2(1310)$ meson ($J^P = 2^+$).

3.4 Cross-section of Unstable Particles

Coherent diffraction on nuclei has been used as a tool for measuring the cross-section of the produced states on the nucleons of the nucleus. In this application the nucleus acts both as a generator of particle and as a target. Let us first consider the elastic reaction $h + A \to h + A$ in the hypothesis that the thickness function $T(\vec{s})$ is slowly varying in comparison with the h-nucleon profile $\Gamma(\vec{s})$. The corresponding phase is obtained by introducing equation 9a and the optical theorem in equation 22:

$$i\Delta_A(\vec{a}) \approx -\sigma_t(1-i\rho)\int_{-\infty}^{+\infty} dz\, \rho(\vec{a},z)/2. \qquad 29.$$

When the real part of the h-nucleon scattering amplitude is zero ($\rho=0$), this expression has a very intuitive meaning: the attenuation introduced by the nucleus in the probability of finding the hadron h at impact parameter $\vec{a}$ just behind the nucleus is proportional to the total cross-section and to the thickness of nuclear matter traversed. In the diffractive process

$h + A \rightarrow h' + A$, particle h survives up to a depth z in the nucleus and the diffractive state h' propagates from this point onward. The overall amplitude for production of the state h' off the nucleus contains the phase factor 29 describing the attenuation of the incident wave and in addition a phase factor containing the total cross-section σ_M for h'-nucleon scattering together with the corresponding real to imaginary ratio ρ_M. Details may be found in the article by Kölbig and Margolis (51). The only point we intend to stress here is that, by measuring the differential cross-section for coherent production of a state of mass M as a function of the mass number A, it is possible to determine the total cross-section of this unstable state on nucleons because, even though the state decays very quickly, it does not have time to vary appreciably while still inside the nucleus.

The curves of Figure 4B represent best fits to the data in which the total cross-section σ_M was left as a free parameter (15-17). The same collaboration has performed phase-shift analysis of the produced three pion system, so as to derive the total cross-section for states of definite spin and parity (18). The results are summarized in Table 1 together with data from other experiments. It is most important to remark that, with the exception of the $0^-(\pi^-\pi^-\pi^+)$ state, all cross-sections are of the same order of magnitude as the cross-sections of stable hadrons. These experiments have tought us the very important fact that such states, usually seen as composite systems, propagate in the nucleus as single hadrons. For detailed discussions of the meaning of this discovery we refer to the literature (53-56). For completeness in Table 1 we have also collected data obtained by studying the coherent photoproduction of vector mesons. In subsection 5.7 we shall show that this is indeed a diffractive process. In this case also, we have to refer to the literature for more details (57, 58).

Table 1. Total cross-sections of unstable hadronic systems on nucleons obtained by measuring coherent production on nuclei

Reaction	P_L (GeV/c)	State	Mass (GeV)	σ_M (mb)	Ref.
$\pi^- A \to \pi^-\pi^-\pi^+ A$	15.1	$(\pi^-\pi^-\pi^+)$	$1.0 < M < 1.2$	23 ± 1.5	17
$\pi^- A \to \pi^-\pi^-\pi^+ A$	15.1	$(\pi^-\pi^-\pi^+) J^P = 0^-$	$1.0 < M < 1.2$	49 ± 8	18
$\pi^- A \to \pi^-\pi^-\pi^+ A$	15.1	$(\pi^-\pi^-\pi^+) J^P = 1^+$	$1.0 < M < 1.2$	15.8 ± 1.4	18
$\pi^- A \to 3\pi^- 2\pi^+ A$	15.1	$(\pi^-\pi^-\pi^-\pi^+\pi^+)$	$1.5 < M < 1.9$	17 ± 8	15
$K^+ A \to K^+\pi^+\pi^- A$	13	$(K^+\pi^+\pi^-)$	$1.0 < M < 1.4$	26 ± 2	20
$pA \to p\pi^+\pi^- A$	22.5	$(p\pi^+\pi^-)$	$1.4 < M < 1.6$	24 ± 3	40
$pA \to p\pi^0 A$	22.7	$(p\pi^0)$	$1.3 < M < 2$	33 ± 7	52
$\gamma A \to \pi^+\pi^- A$	<7	ρ^0	0.77	26.7 ± 2	57
$\gamma A \to K^+K^- A$	<5	ϕ^0	1.02	12 ± 4	57

4. DIFFRACTION SCATTERING IN HADRON-HADRON COLLISIONS

4.1 Characteristic Features of Hadronic Diffractive Phenomena

Our previous discussion of diffraction phenomena for optical waves and for hadronic waves on nuclei allow us now to abstract those features that a particular final state produced in a hadron-hadron collision has to present in order to be classified under the heading "diffractive phenomenon".

The range of strong interaction is of the order of 1 fm and the short wave length condition is satisfied if the laboratory momentum of a projectile hadron impinging on a nucleon is larger than ~ 5 GeV/c (section 2.3). Figure 9A shows that at these momenta the inelastic cross-sections of the usual six stable particles on protons are of the order of the area of a disc 1 fm in radius: $\sigma \approx 30$ mb. According to equation 13 these large values may be obtained only if the hadron-hadron profile function is essentially real and, for small impact parameters, is not very far from the maximum allowed value: $\Gamma(0) \approx 1$. This is enough to "drive" shadow phenomena and one is left with the problem of recognizing them. Let us consider the inelastic two-body reaction

$$a + b \to c + d \ ,$$

representing the interaction of the projectile hadron a with the target hadron b that produces two hadronic systems c and d, which in general are observed as multiparticle final states. The systems c and d are assumed well separated and associated with well-defined quantum numbers. This reaction is labelled "diffractive process" if the following key features are observed.

(a) The differential cross-section has a pronounced forward peak whose slope is of the order of 5-10 GeV^{-2} (equation 16). Note however, that if for some dynamical reasons the process is peripheral in the impact parameter $\vec{a}$,

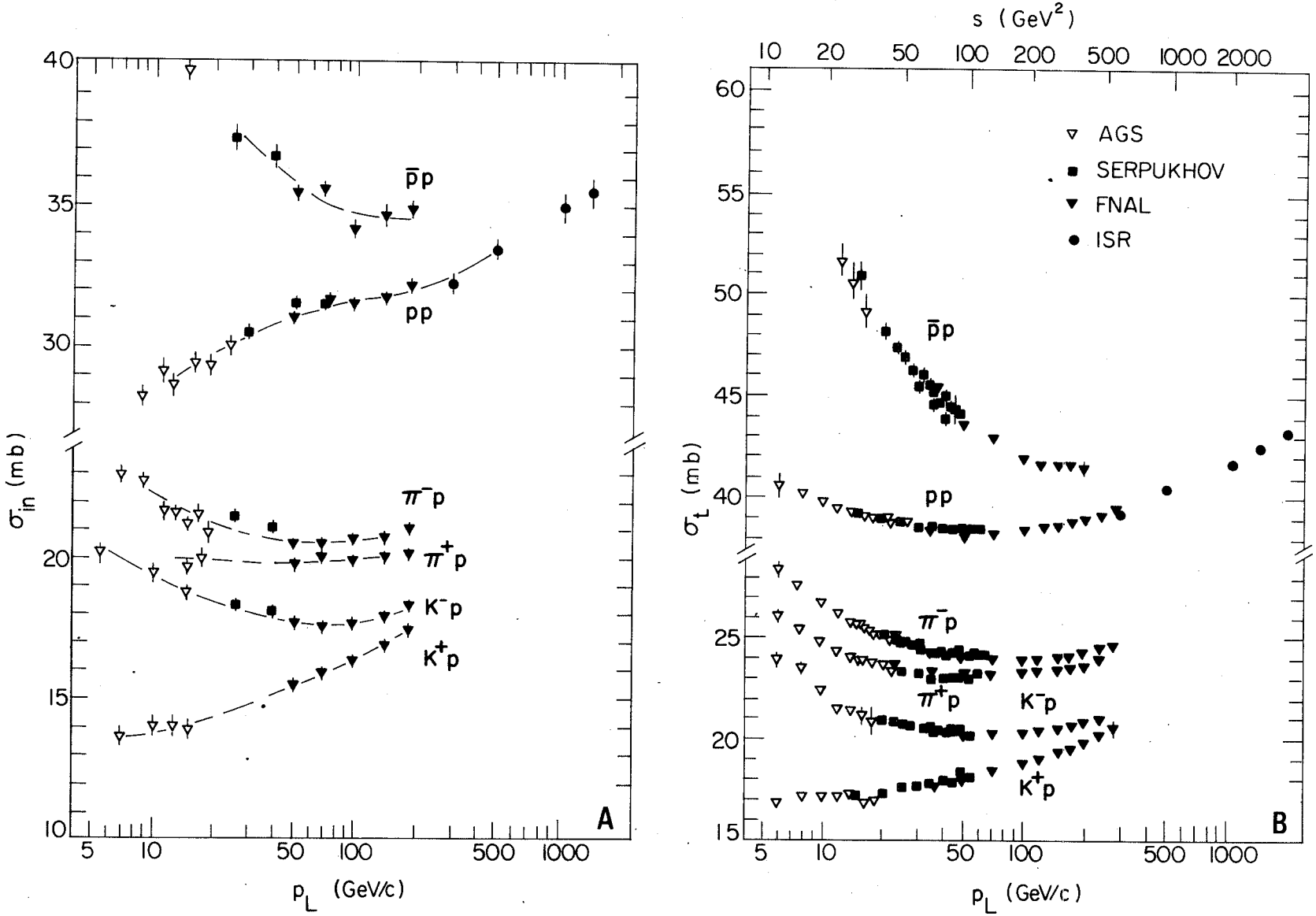

Figure 9 (A) Inelastic cross sections σ_{in} of six stable or metastable hadrons or protons. The curves are only to guide the eye. The values of σ_{in} are obtained by subtracting the elastic cross section σ_{el} from the measured values of σ_t.

(B) Total cross sections σ_t of the same six hadrons on protons (59a-59f, 66-67).

the forward slope may be substantially larger. (Compare Figures 2B and 2A).

(b) The integrated cross-section is a "slowly" varying function of the momentum of the projectile. This follows from the fact that the hadron-hadron profile function must vary little with the momentum, as indicated by the slow variation of the inelastic cross-section (Figure 9A). What is meant by "slowly" cannot be stated in absolute terms but may be defined only in comparison with the "fast" energy variation of cross-sections which are certainly not of diffractive type. Typically they vary as inverse powers of s, the square of the centre-of-mass energy. In this context a "slow" variation means, for instance, a logarithmic dependence on s.

(c) The systems c and d have the same intrinsic quantum numbers as that of the hadrons a and b, respectively. Their spin and the parity may be different but are a priori expected to follow the Gribov-Morrison rule of equation 28. Note that the association of c with a and d with b is unambiguous because of the large forward peak required by condition (a).

(d) The cross-sections of processes initiated by a hadron and its antihadron behave similarly as a function both of momentum transfer and of laboratory momentum. This is expected from the fact that the range of strong interactions is practically universal and that the inelastic cross-sections of a hadron is numerically close to the cross-section of its antiparticle (Figure 9A). Annihilations contribute a relatively small part of absorption.

(e) The incoming momentum has to be large enough to allow for coherence over the dimensions of the hadron. According to equation 18, this implies a threshold for the laboratory momentum p_L needed to coherently produce on the target of mass m a state of mass M:

$$p_L \gtrsim 2.5\ (M^2 - m^2), \qquad 30.$$

where momentum and masses are measured in GeV and we have taken R=1 fm. As a numerical example, diffractive excitation of a 3 GeV system, even if allowed by other selection rules, will be depressed if p_L is less than about

25 GeV/c, while for M = 10 GeV p_L must be of the order of 250 GeV/c.

In the case of diffractive elastic scattering one also expects the scattering amplitude to be mainly imaginary, at least in the forward direction. This happens if the interaction is essentially absorptive, so that the phase is imaginary and the profile function is real.

4.2 Exchange Picture of Diffraction

The optical picture of high energy elastic scattering leads to a semi-classical approach which is very different from the usual quantum field treatment so successful in electrodynamics. In this framework the basic process is of an exchange nature, the two interacting particles exchanging quanta of a field they are coupled to. This is the well-known picture of Coulomb scattering, where a photon is exchanged. With strong interactions this is the Yukawa theory, with pion exchange as the basic interaction between two colliding hadrons. The very nature of strong interactions does not allow, however, a perturbative expansion. The picture is even more complicated because of the great number of mesons which can be exchanged. Still the Chew and Frautschi application of Regge's ideas (60) allows to use a relatively simple exchange picture to the description of hadron collisions, which is in fact the result of a tremendous averaging over elementary processes. It is out of question to provide here an introduction to Regge models, for which we refer the reader to recent reviews (61,62). We shall merely say that, once a reaction can be labelled as proceeding through the exchange of a particular set of quantum numbers, the corresponding scattering amplitude can be approximated as

$$R(s,t) = \sum_i \gamma^i_{ab}(t)\ \gamma^i_{cd}(t)\ \eta_i(t)\ (s/s_o)^{\alpha_i(t)} \qquad 31.$$

where s is the square of the centre-of-mass energy ($s \approx 2\ p^a_L\ m_b$). Each term in the sum corresponds to the exchange of a "Regge trajectory", which connects the spin J and the masses M of particles, having the quantum numbers exchanged in the process, through the relation $J = \alpha(M^2)$. It is this

trajectory, continued from positive arguments (M^2) to negative ones (t), that fixes the phase and the energy dependence of the amplitude. The factors $\gamma^i_{ab}(t)$ and $\gamma^i_{cd}(t)$ may be interpreted as coupling constants of the exchanged trajectory with the "upper" line, describing the transition $\underline{a} \to \underline{b}$, and the "lower" line, describing $\underline{c} \to \underline{d}$. The function $\eta(t)$ is called "signature factor" and has the explicit form

$$\eta(t) = \left\{\tau + \exp\left[-i\pi\,\alpha(t)\right]\right\}/\sin\pi\alpha(t) \qquad 32.$$

It brings in the amplitude poles due to the vanishing of the denominator for odd (even) integer values of $\alpha(t)$ according to the value +1 or -1 taken by the signature τ. In field theory the exchange of a particle gives rise to a pole in the amplitude. The signature factor is indeed producing this effect. The scale parameter s_o is of the order of 1 GeV^2.

Introducing the relativistic amplitude

$$F(s,t) = 4\pi\, s\, f(q)/k \qquad 33.$$

the full amplitude for the process a + b → c + d may be written

$$F(s,t) = R(s,t) + Z(s,t)\ , \qquad 34.$$

where R sums the contributions from a very few Regge trajectories and Z stands for the corresponding remainder. One may now summarize over a decade of Reggeology saying that, whenever R is large, R alone, with the properties associated with equation 31, meets an impressive amount of data and, as shown by the recent Fermilab results, is furthermore successful over a tremendous energy range. However, one is still lacking a satisfactory form for the remainder Z. This is an important drawback, in particular whenever R is small. A specific example of a large R(t) is provided by pion-nucleon charge exchange ($\pi^- p \to \pi^0 n$), where the exchange trajectories have to carry one unit of charge and one unit of isospin and be even under G parity. One known meson meets all these properties, the ρ-meson. The

data may be fitted with a single term of equation 31 in the ranges $5 < p_L < 100$ GeV/c and $|t| \lesssim 1$ GeV^2 with a trajectory of the form

$$\alpha(t) = \alpha_0 + \alpha' t \ , \qquad 35.$$

when $\alpha_0 \approx 0.5$ and $\alpha' \approx 0.7$ GeV^{-2} (Figure 10). This trajectory extrapolates well to the masses of the ρ and of the g mesons. This success is really impressive and is not isolated. One may also quote η production in πp collisions, K_S regeneration from K_L, total cross-section differences. However when the Regge pole amplitude is small, the remainder Z may not be neglected, as indicated for instance by the presence of a sizeable polarization in $\pi^- p$ charge exchange. (61, 64).

It is now tempting to assess the predicting power of a similar approach when it comes to elastic scattering, which is by all standards a large amplitude. In such a case one may tentatively introduce a leading Regge amplitude as

$$R^P(s,t) = \gamma^P_{aa}(t)\ \gamma^P_{bb}(t)\ \eta_P(t)\,(s/s_o)^{\alpha_P(t)}. \qquad 36.$$

The properties of the Regge trajectory which would give an a priori satisfactory form for a diffractive amplitude are readily obtained. The trajectory is associated with the exchange of the quantum numbers of the vacuum. It should be even under C- and G-conjugation and with positive signature. Since the optical theorem reads $s\,\sigma_t = \mathrm{Im}\,F(s,0)$, by neglecting the remainder Z(s,t) the total cross-section becomes .

$$\sigma^{ab}_t = \gamma^P_{aa}(0)\gamma^P_{bb}(0)\ \mathrm{Im}\left[\eta_P(0)\right] s^{\alpha_P(0)-1}\, s_o\,(s/s_o)^{\alpha_P(0)-1} + \sum_i \gamma^i_{aa}(0)\gamma^i_{bb}(0)\ \mathrm{Im}\left[\eta_i(0)\right] s_o\,(s/s_o)^{\alpha_i(0)-1} \qquad 37.$$

The sum stands for the contribution of the non-leading trajectories, which have $\alpha_i(0) < \alpha_P(0)$. They could be neglected asymptotically ($s \to \infty$). The first term contributes a constant cross-section if $\alpha_P(0) = 1$, which implies

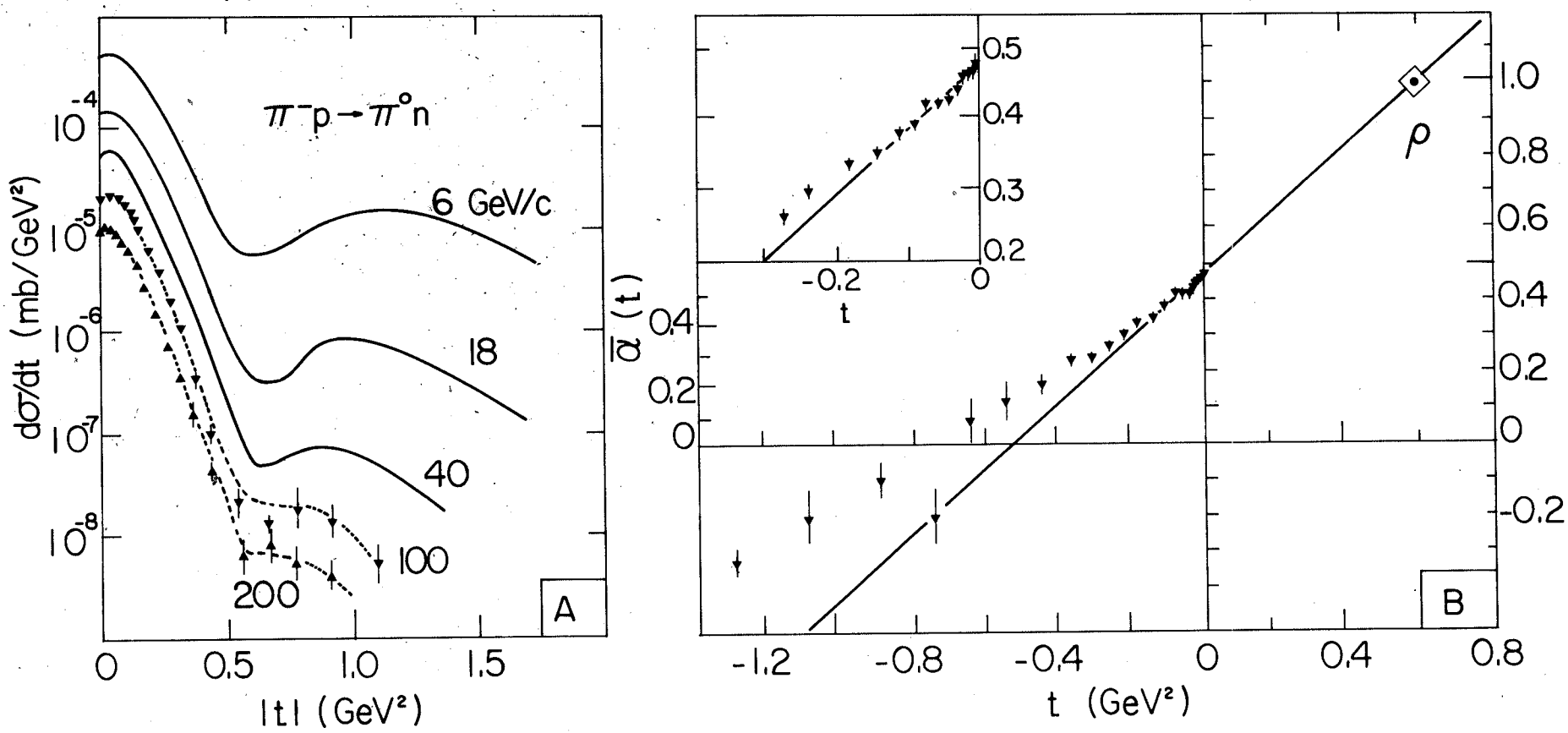

Figure 10 Compilation of data on the charge exchange reaction $\pi^- p \to \pi^o n$.

(A) A sample of data on the differential cross section. The curves at lower energies are taken from Diddens review paper (63a). The points are some of the recent data of FNAL (63b).

(B) Effective trajectory $\bar{\alpha}(t)$ derived from the FNAL data (63b). The straight line goes through the ρ and g meson masses. The inset shows the details close to t = 0.

$\eta_P(0) = i$. This contribution is by construction the same for particle and antiparticle scattering off the same target (it is even under C). Since it dominates asymptotically, it satisfies the Pomeranchuk theorem, which states that the cross-section of a particle and antiparticle off the same target are asymptotically equal (65). For this reason the trajectory with $\alpha_P(0) = 1$ is called Pomeron.

Since the findings of the CERN Intersecting Storage Rings (66,67) and of Fermilab (68,69) we know that the total cross-sections increase with s (Figure 9B). Thus the leading term of the cross-section should include at least extra logarithms in s which are not present in the Regge expansion of equation 37. For the time being we shall consider the Pomeron amplitude only as a simple first approximation to the true amplitude describing shadow phenomena in hadron-hadron collisions. We then point out two consequences which are proper to the exchange picture of diffraction processes.

First, since $d\sigma/dt = |F|^2/(16\pi s^2)$, if Pomeron exchange with $\alpha(0) = 1$ dominates, by using the parametrization of equation 35 one expects

$$d\sigma/dt = \left[\gamma^P_{aa}(t)\ \gamma^P_{bb}(t)\right]^2 \exp\left[2\alpha'_P t\ \ell n(s/s_o)\right]/(16\pi s_o^2) \qquad 38.$$

This expression implies that the slope b of the forward elastic scattering increases proportionally to $\ell n\ s$, i.e. the diffractive peak shrinks with energy. If,as successfully done, the coupling constants γ^P_{aa} and γ^P_{bb} are parametrized by exponentials in t, equation 38 also implies a profile function which is gaussian in impact parameter (Figure 2D) with an interaction radius which increases logarithmically with energy: $R^2 = R_o^2 + 4\alpha'_P\ \ell n(s/s_o)$ (equation 16). Since the total cross-section is constant, at the same time the central value of the profile has to decrease: $\Gamma(0) \propto 1/\ell n\ s$. Clearly this prediction is very far from any black disc analogy.

Second, the Pomeron amplitude contains the product $\gamma_{aa}^{P}\ \gamma_{bb}^{P}$, which implies factorization properties which are also not obvious in an optical picture. For instance consider the proton diffractive excitation initiated by a proton, a pion or a Kaon. The factorized Pomeron amplitude gives $\sigma(pp \to pN^*)/\sigma(pp \to pp) = \sigma(\pi p \to \pi N^*)/\sigma(\pi p \to \pi p) = \sigma(Kp \to KN^*)/\sigma(Kp \to KP)$. 39. Similarly

$$[\sigma(pp \to pN^*)]^2 = 4\sigma(pp \to pp)\ \sigma(pp \to N^*N^*)\ . \qquad 40.$$

Such relations should hold for differential as well as total cross-sections.

In the following these two predictions and the general features of diffraction processes discussed in the previous section will be compared with the experimental data.

4.3 Elastic and Total Cross-Sections

Examples of forward hadron-proton differential cross-sections are plotted in Figures 11A and 11B. Besides the almost exponential behaviour in t, we remark a "cross-over" point at $|t| \simeq 0.2\ GeV^2$ between the differential cross-sections of particles and antiparticles. This effect may be interpreted geometrically as a consequence of the fact that antiparticles are more extended than particles in impact parameter space, so that both the forward cross-section and the slope are larger for antiparticle-hadron than for particle-hadron interactions. From the exchange point of view, since the Pomeron is even under charge conjugation, its exchange gives equal particle and antiparticle cross-sections. Thus the cross-over phenomenon tells something about the other exchanged Regge trajectories. This point has been discussed extensively in the literature (71-73) and we do not dwell upon it here. The πp and Kp total cross-sections are definitely different at $p_L \gtrsim 200$ GeV/c (Figure 9B). This implies different forward elastic cross-sections, so that at t=0 the Pomeron, if it acts as an isospin

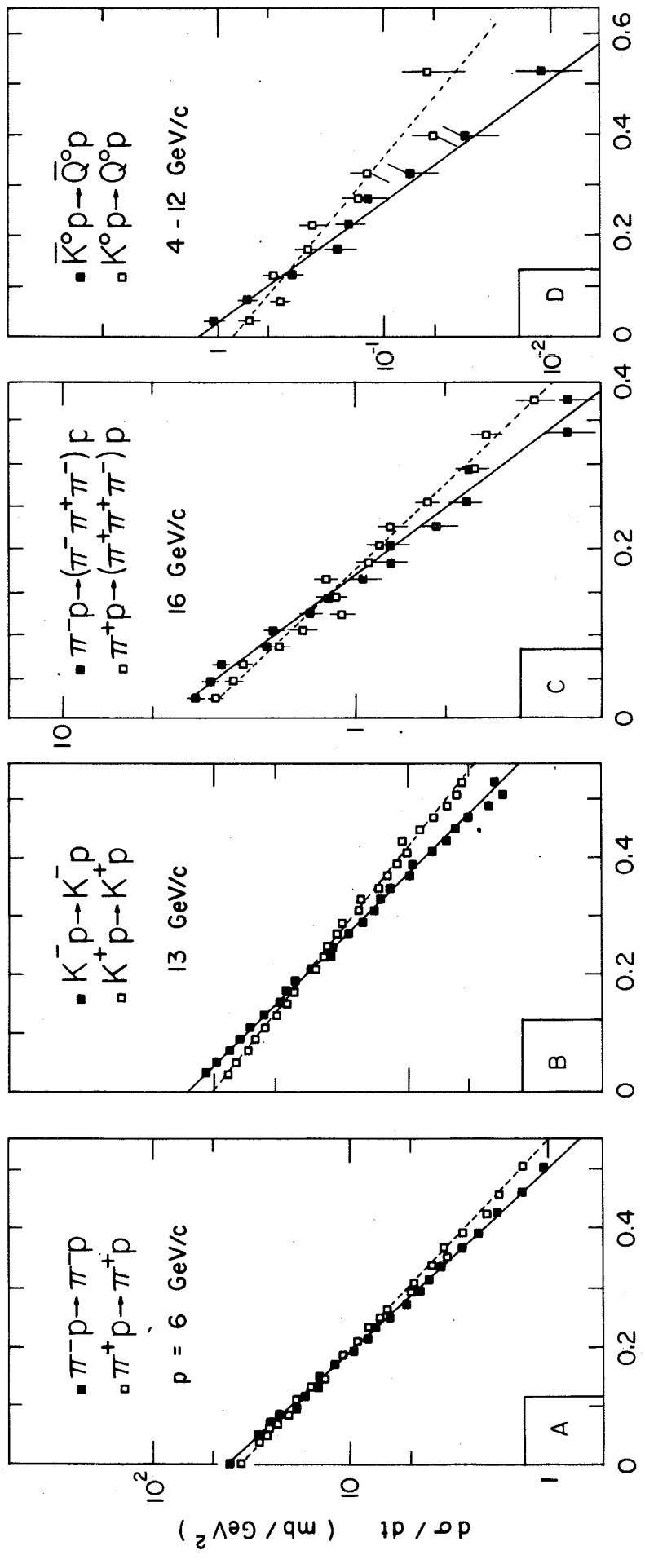

Figure 11 (A, B) Examples of forward hadron-proton elastic cross sections (70a, 70b). Note the cross-over phenomenon.
(C, D) The same effect appears in diffractive processes (70c, 124).

singlet, does not act as a unitary singlet (i.e. as a singlet under the SU(3) symmetry group of strong interactions). This however seems to change with momentum transfer, since there are indications from Fermilab that the differential cross-section for πp and Kp eventually merge for $|t| \gtrsim 0.3$ GeV^2 (74). This is connected with the long debated Pomeron-f analogy which we do not discuss here.

Information on the secondary exchanges are also obtained by measuring the polarization parameter P in elastic scattering and the differences between particle and antiparticle cross-sections. In the first type of experiment, hadrons are scattered on polarized protons. The technique introduced at the PS by the CERN-Pisa collaboration (75,76) has been recently used at higher energy by the Saclay-Serpukhov-Dubna-Moscow collaboration working at Serpukhov (77). The energy dependence of the parameter P in $\pi^{\pm}p$ scattering at fixed t may be fitted by the interference of a Pomeron amplitude of slope $\alpha'_P = 0.27$ GeV^2 with a secondary "effective" trajectory of the form $\bar{\alpha} = 0.52 + 0.93\ t$ (77). The difference between particle and antiparticle cross-sections gives also information on the effective intercept $\bar{\alpha}_0$ of the secondary trajectories (equation 37). The data plotted in Figure 12 give $\bar{\alpha}_0 \simeq 0.5$, in agreement with the masses of the mesons which can be exchanged and with the polarization data. This two types of experiments are interesting to combine since the latter one is only sensitive to the imaginary part of the non-flip secondary exchange contribution, while in the former one, it is the real part of the spin flip secondary exchange contribution which mainly matters. In conclusion, the available data indicate that the secondary contributions have an effective intercept $\alpha_0 \approx 0.5$, so that they decrease about as $s^{\frac{1}{2}}$ with respect to the almost constant Pomeron cross-section.

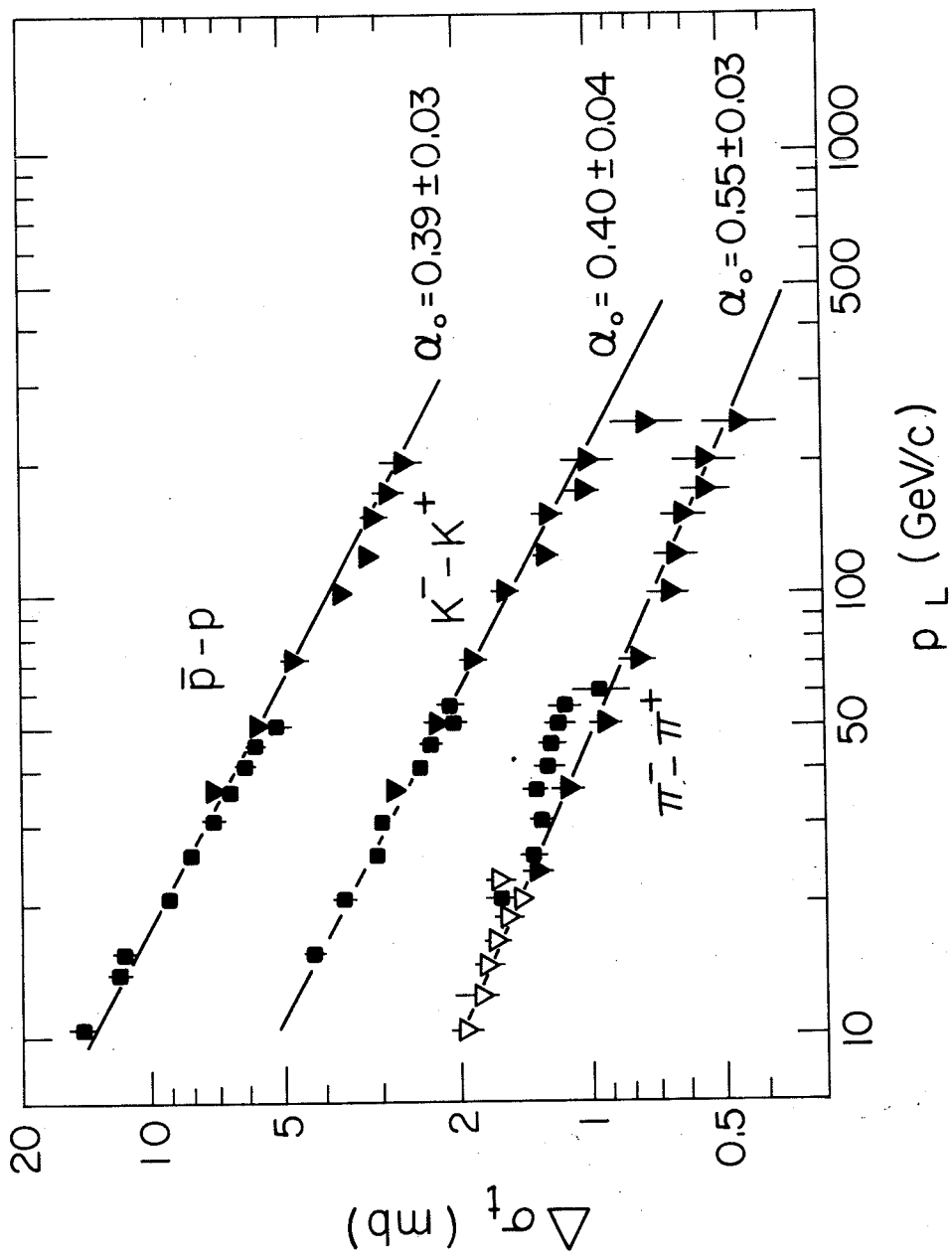

Figure 12 Energy dependence of the difference of antiparticle and particle cross sections on protons (59e).

Proton-proton elastic scattering is very well known in large intervals of energy and momentum transfer. A compilation of data is shown in Figure 13. With increasing laboratory momentum a typical diffraction minimum develops around $|t| = 1.4$ GeV^2. It occurs as the momentum increases between 100 and 200 GeV/c. The change between the kink appearing at lower momenta and the dip is presumably due to the gradual vanishing of the real part at these t-values, as it looses the contribution of the secondary Regge trajectories. The CERN-Hamburg-Orsay-Vienna collaboration working at the CERN Intersecting Storage Rings has shown that the position of the diffraction minimum changes from $|t| = (1.44 \pm .02)$ GeV^2 to $(1.26 \pm .03)$GeV^2 when the centre-of-mass energy passes from 23 to 62 GeV, i.e. when p_L increases from 300 to 2000 GeV/c (79). This (14 ± 3) % change of the position of the minimum is equal, within the errors, to the (11 ± 2) % increase of the total cross-section and to the (12 ± 2) % increase of the inelastic cross-sections which are observed in the same energy interval (Figure 9). From an optical point of view such a coincidence is easily understood, assuming that the profile function is real and depends upon the incoming momentum only through a scale dilatation of its argument: $\Gamma(a,p_L) = \Gamma[a/R(p_L)]$. When the momentum increases the value at a = 0 remains constant, while the radius $R(p_L)$ expands. This form of "geometrical scaling" (80, 81) implies that σ_t and σ_{in} are both proportional to $R^2(p_L)$, so that the data indicate that in the ISR energy range the radius of the profile function increases by ~6%. Since b is proportional to R^2, the slope should then increase by 12%. The data plotted in Figure 14A give (13 ± 3)%.

The proton-proton forward peak shrinks with energy and the slope b at $\langle t \rangle \simeq 0.05$ GeV^2 increases logarithmically with s, as predicted by the Pomeron amplitude of equation 38. A fit to the data of Figure 14A above $p_L \sim 30$ GeV/c

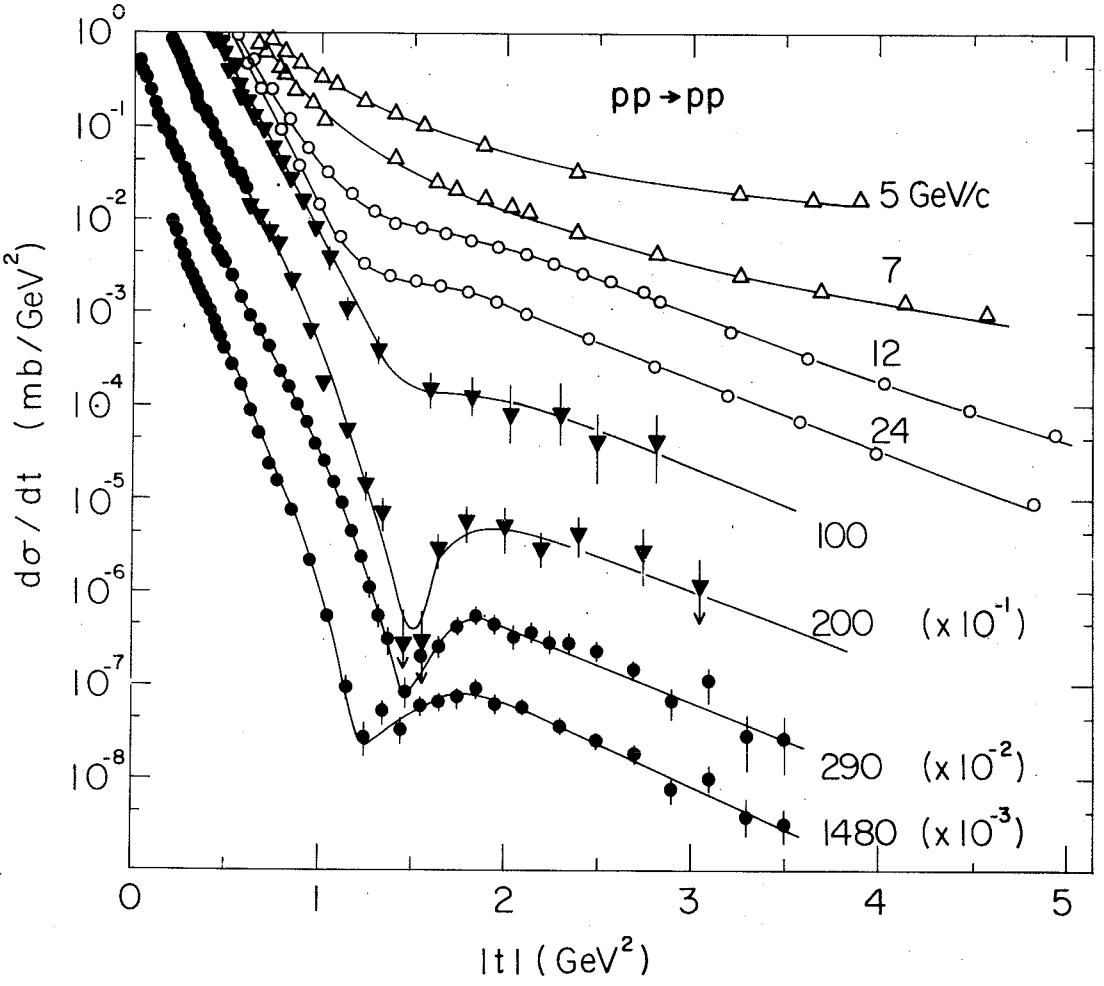

Figure 13 Compilation of proton-proton differential cross sections. The data are from Berkeley (5-7 GeV/c, 78a), PS (78b), FNAL (78c) and ISR (78d). The recent data of the CERN-Hamburg-Orsay-Vienna Collaboration indicate that there is no other minimum up to $|t| \approx 8$ GeV^2 (79).

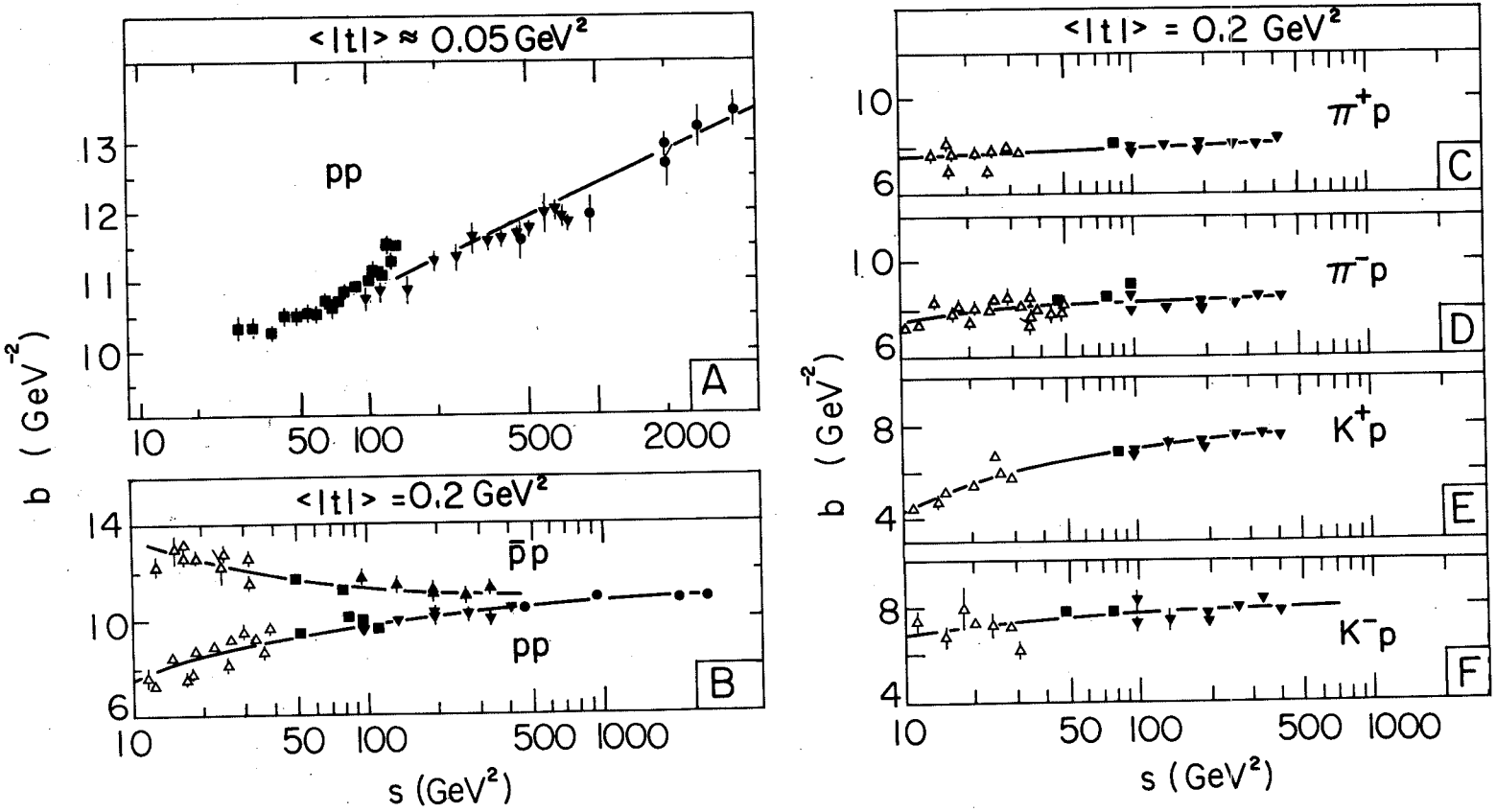

Figure 14 Forward slopes of the elastic scattering cross-section.

(A) Proton-proton slope at a very small average momentum transfer (82a-82-d, 84). The line represents the relation b = (8.0 + 0.62 ℓns) where s is measured in GeV^2.

(B-F) Slopes measured for an average momentum transfer $\langle t \rangle \approx 0.2\ GeV^{-2}$ (82e-82j).

gives for the Pomeron slope $\alpha_p' \approx 0.30$ GeV^{-2}. This value agrees with the polarization measurement quoted above and is much smaller than ~ 0.8 GeV^{-2}, characteristic of all the other Regge trajectories.

Slopes computed at an average momentum transfer $\langle t \rangle = 0.2$ GeV^2 are also plotted in Figure 14. In the proton-proton channel the slope decreases passing from $\langle t \rangle = 0.05$ GeV^2 to $\langle t \rangle = 0.2$ GeV^2. This reflects the sharp rise of the differential cross-section for momentum transfers smaller than ~ 0.1 GeV^2 (84). The compilations of Figure 14 show that, while the slope of $\pi^- p$ and $K^- p$ elastic scattering is almost energy independent, the $\pi^+ p$ and the $K^+ p$ slopes increase with energy, i.e. their forward elastic peak shrinks. Indeed one expects strong constructive interference between the first and the second term in expansion 37 for $K^- p$, but practically none for $K^+ p$.

Total cross-sections for the usual six channels are plotted in Figure 9A. For a discussion of the relative values of these cross-sections and their energy dependence in terms of the quark model we refer to the recent review by Wetherell (59a). A comparison between the energy dependences of the total cross-sections (Figure 9) and the slopes (Figure 14) indicates that the channels whose total cross-section varies more rapidly show also a faster increase of the slope. This is quantitatively shown in Figure 15, where the ratios b/σ_t are plotted versus s (85,86). The fact that this ratio stays constant with energy is in agreement with the hypothesis that geometrical scaling is qualitatively valid in all six channels. The same conclusion may be reached by considering the energy dependence of the ratios σ_{el}/σ_t plotted in Figure 16. This figure demonstrates that at large enough energies these ratios are practically constant. It also shows that in all channels the ratio σ_{el}/σ_t is very far from 1/2, which is the value expected for a black disc (equations 13 and 14). (For the proton-proton case the fact that the profile function is very far from a black disc appears very clearly in the inset of Figure 3C.)

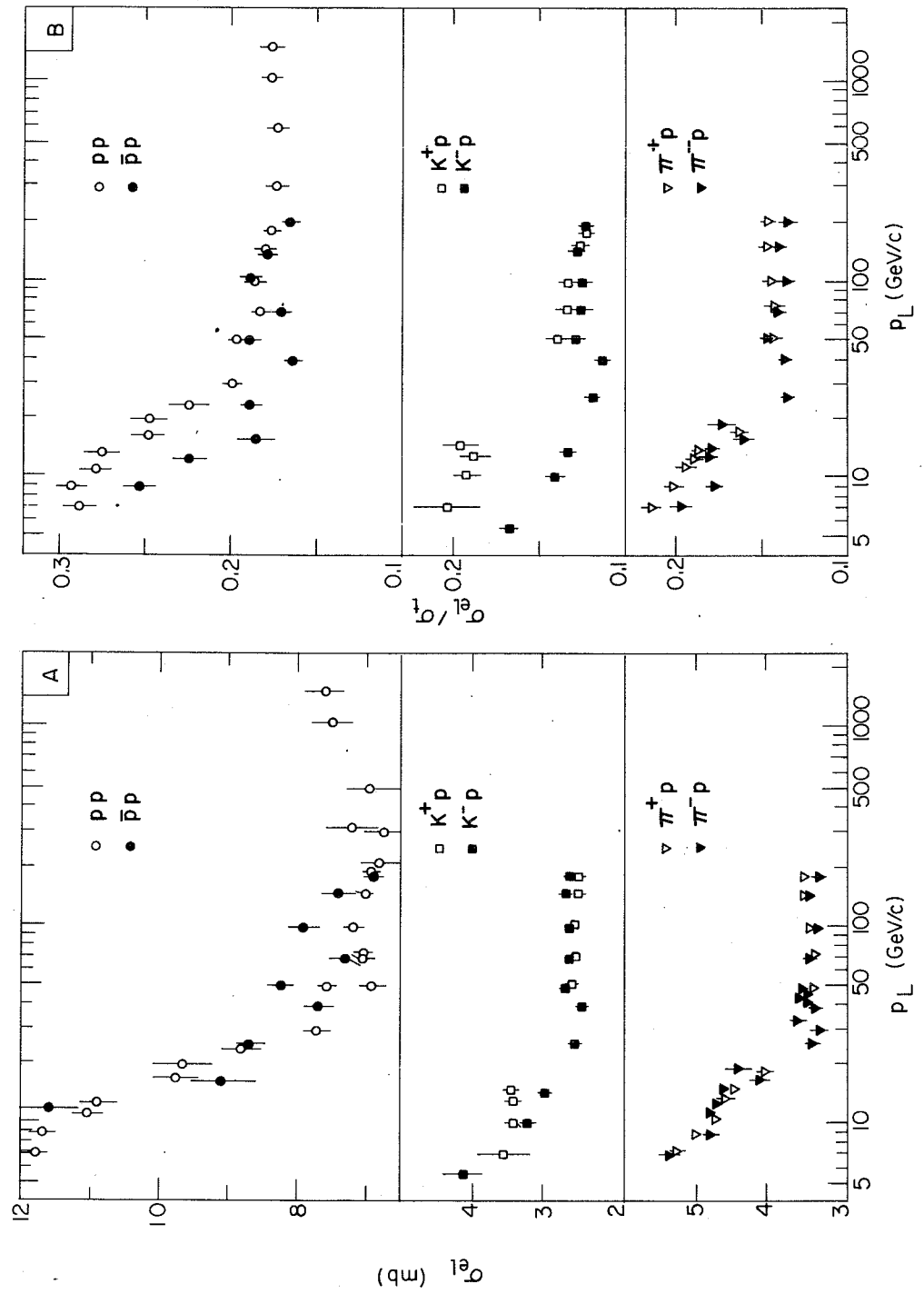

Figure 16 (A) Compilation of elastic cross sections (87a-87c). The curves are just to guide the eye.
(B) Energy dependence of the ratio σ_{el}/σ_t.

imaginary part of the Coulomb amplitude are easily introduced (89), and the measurement of elastic scattering at very small values of $|t|$ gives information on ρ. The experimental data are plotted in Figure 17. It is seen that at high energies the parameter ρ is small, i.e. the nuclear amplitude is mainly imaginary, as expected for a diffractive process driven by a large absorption.

In optics the real part of the refractive index of a medium at a given frequency may be expressed as an integral over a function of the imaginary part of the refraction index extended to all frequencies. Similar dispersion relations, consequence of the causality principle, connect the real and imaginary parts of the nuclear scattering amplitude. Since the imaginary part of the forward amplitude is proportional to the total cross-section, at any given energy the value of ρ may be expressed as an integral of the total cross-section for particle and antiparticle over the whole energy range (90, 91). In practice the value of ρ is mainly sensitive to the local derivative of the total cross-section, since to a first approximation the result of the dispersion relation may be written in the form (92)

$$\rho \approx \frac{1}{\sigma_t}\left[\operatorname{tg}\left(\frac{\pi}{2}\frac{d}{d\ \ell n\ s}\right)\right]\sigma_t = \frac{1}{\sigma_t}\left[\frac{\pi}{2}\frac{d}{d\ \ell n\ s} + \frac{1}{3}\left(\frac{\pi}{2}\right)^3 \frac{d^3}{d\ \ell n\ s^3} + \ldots\right]\sigma_t(s). \quad 42.$$

This expression assumes that the scattering amplitude is even under crossing, as it should be asymptotically. It indicates, for instance, that if the cross-section rises at the maximum rate allowed by the Froissart bound (93), i.e. as $\ell n^2 s$, the parameter ρ approaches zero as $1/\ell n s$ from positive values. This statement is indeed a much more general consequence of field theory when the total cross-section increases asymptotically. It is the Khuri-Kinoshita theorem (94). Figure 17 shows that ρ indeed becomes positive in all channels in the range $100 \leq p_L \leq 200$ GeV/c in agreement with the observed rise in the total cross-sections (Figure 9) and the Khuri-Kinoshita

theorem. What happens to the real part at even larger energies is a very relevant question in the field of elastic diffraction, because, as indicated by equation 42, it could give a hint on the higher energy dependence of the total cross-section. At present the CERN-Rome collaboration is performing an ISR experiment which should provide values of ρ in proton-proton scattering up to $p_L \simeq 2000$ GeV/c.

4.5 Unitarity and Diffraction Scattering

Probability conservation implies the unitarity of the S-matrix: $S^\dagger S=1$. By introducing the transition matrix ($S = 1+i\,T$) the unitarity relation reads $i(T-T^\dagger)= T^\dagger T$. Sandwiching this between the initial state $|i\rangle$ of the two colliding hadrons and the outgoing elastic state $|f\rangle$, and using the usual normalization one gets

$$4\pi\ \mathrm{Im}\ f/k = \sum_{m\ el} \langle f|T^\dagger|m\rangle\langle m|T|i\rangle + \sum_{n\ inel} \langle f|T^\dagger|n\rangle\langle n|T|i\rangle. \qquad 43.$$

The left hand side is proportional to the imaginary part of the elastic scattering amplitude. The expression on the right hand side has been obtained introducing in $\langle f|T^\dagger T|i\rangle$ a complete set of states, and then distinguishing the elastic intermediate state $|m\rangle$ from the inelastic ones $|n\rangle$. Equation 43 is diagrammatically represented in Figure 18. It states that the imaginary part of the scattering amplitude receives contributions both from elastic and inelastic intermediate states. Following Van Hove (96), the two terms on the right of the equation 43 are named elastic and inelastic overlap functions. They are function of the momentum transfer t:

$$4\pi\ \mathrm{Im}\ f(t)/k = G_{el}(t) + G_{in}(t). \qquad 44.$$

For t=0 this equation reduces to the optical theorem. Indeed the overlap functions are so normalized that $G_{el}(0) = \sigma_{el}$ and $G_{in}(0) = \sigma_{in}$. If the real part of the elastic amplitudes is negligible, $G_{el}(t)$ which is expressed

by the integral $\int f^*(\vec{q}') f(\vec{q} - \vec{q}') d^3q'$, contains only Imf and equation 44 becomes a non-linear integral equation in $f(\vec{q})$, once the inelastic overlap function is supposed to be known. In this "shadow" approximation the knowledge of the inelastic transition matrix elements $\langle n|T|i\rangle$ allows the calculation of the elastic amplitude. This is the program of all s-channel approaches to high energy elastic scattering: use a model for the inelastic processes to compute the inelastic overlap function and then solve equation 44 for the elastic amplitude. The first step is the most difficult one because the model must specify both the modulus and the phase of the inelastic matrix elements. Physically this is due to the fact that the phase is related to the position in space where the particles are produced (97). Many attempts have been performed along these lines and the main results may be summarized as follows. If the production channels are described by an uncorrelated jet model (96-98), or by a multiperipheral model (99-101) it is impossible to reproduce the slope of the elastic amplitude. This difficulty may be cured by introducing correlations among the produced hadrons (99-101), a phenomenon which is known to be present in production processes.

Above which laboratory momentum is the shadow approximation expected to be a good approximation? Since the integral of the overlap function $G_{in}(a)$ is proportional to the inelastic cross-section, it is natural to look to the energy dependence of σ_{in}. The data plotted in Figure 9A clearly indicate that one has to distinguish two cases. In the pp and K^+p channels the inelastic cross-section rises continuously, while in the others it decreases with the laboratory momentum up to at least 50 GeV/c.

This behaviour is connected with the absence of direct formation resonances in the "exotic" channels pp and K^+p (87c). Thus these two reactions are the most suitable to study shadow effects at not too high

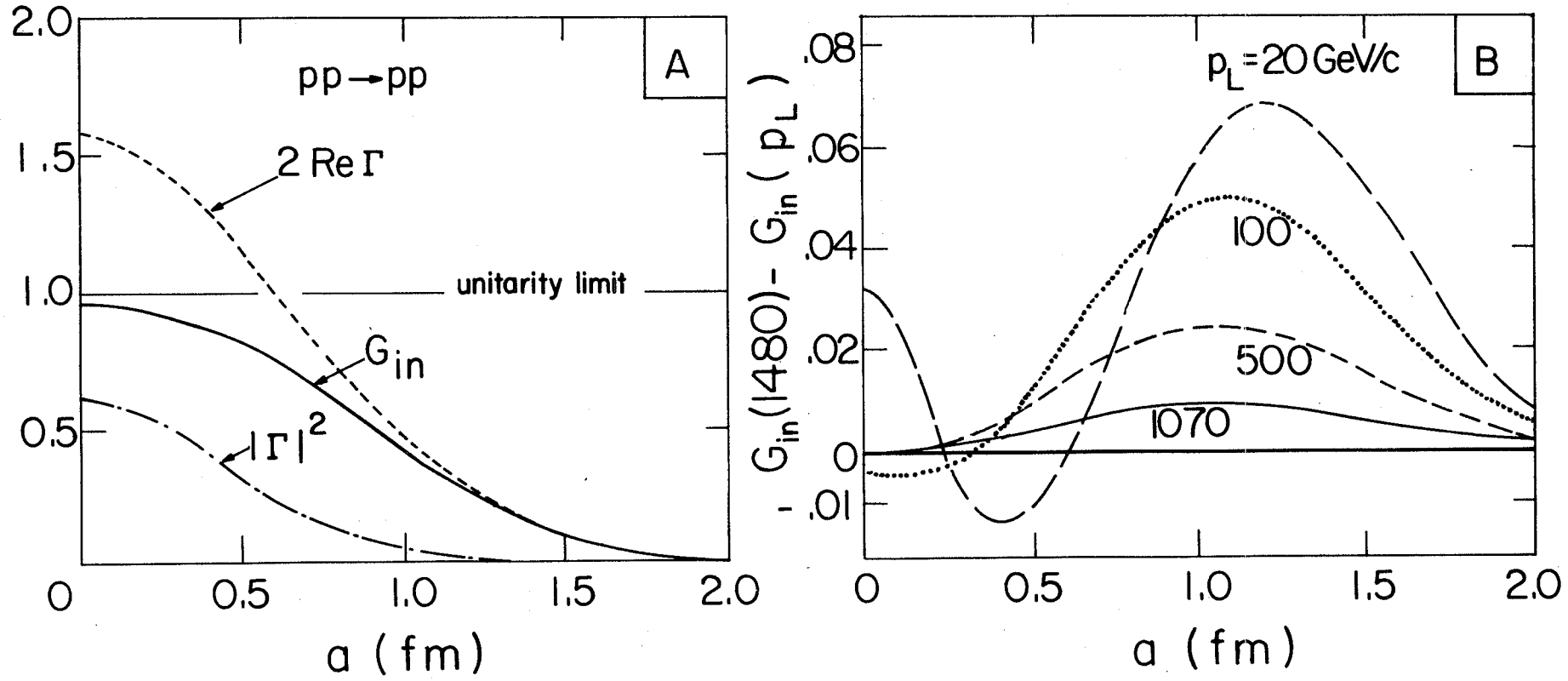

Figure 19 (A) Impact parameter dependence of the inelastic overlap function $G_{in}(a)$ for proton-proton scattering at p_L = 1480 GeV/c. The dashed and dash-dotted curves represent the other two terms appearing in the unitarity conditions of equation 45 (102).

(B) Energy variation of the inelastic overlap integral as computed by Grein et al. (102).

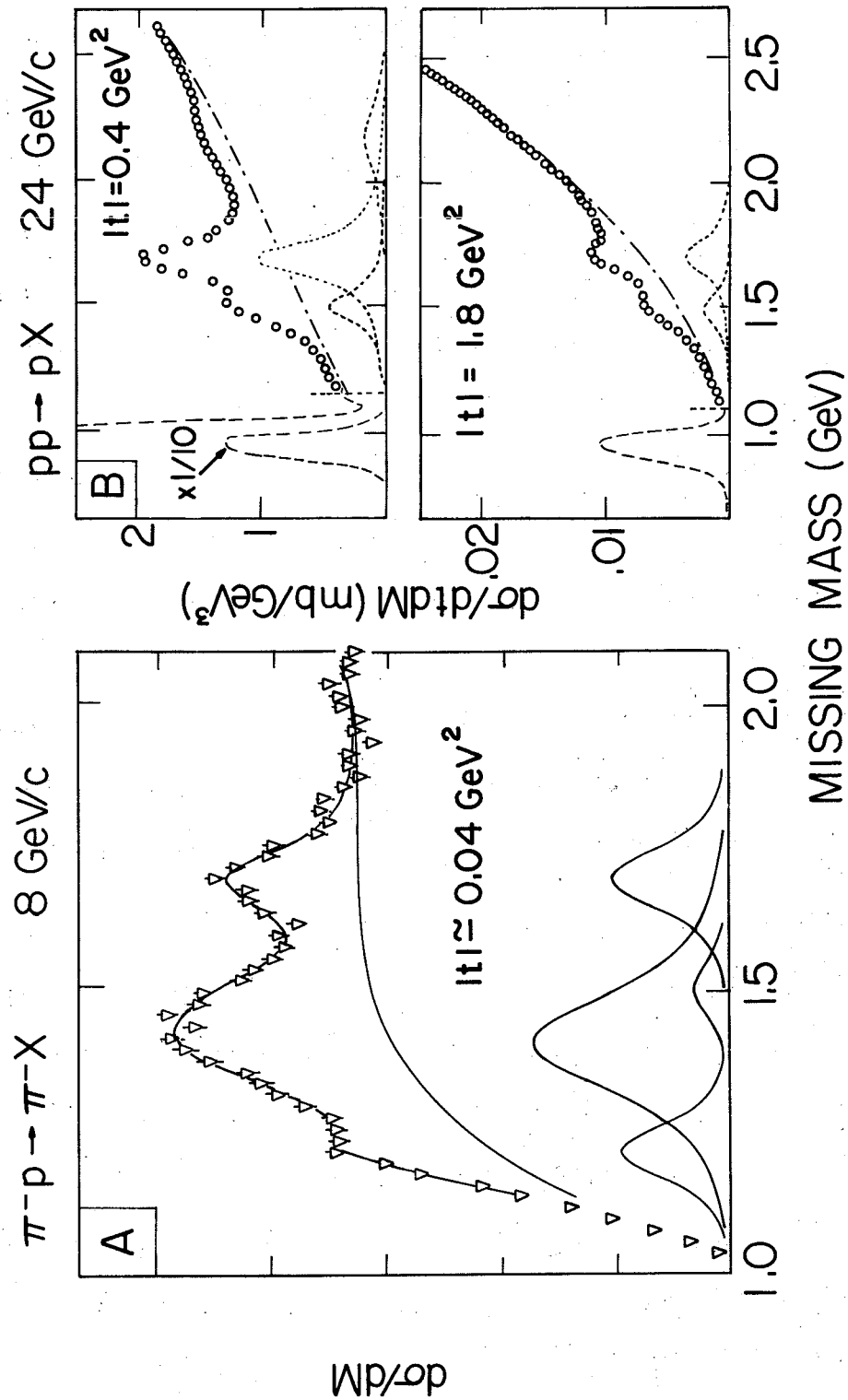

Figure 20 Missing mass spectra for proton dissociation.

(A) AGS data of reference 105.

(B) PS data of reference 78b. The lines represent the results of fits obtained by adding the resonance contribution with Breit-Wigner shape to a smooth continuum.

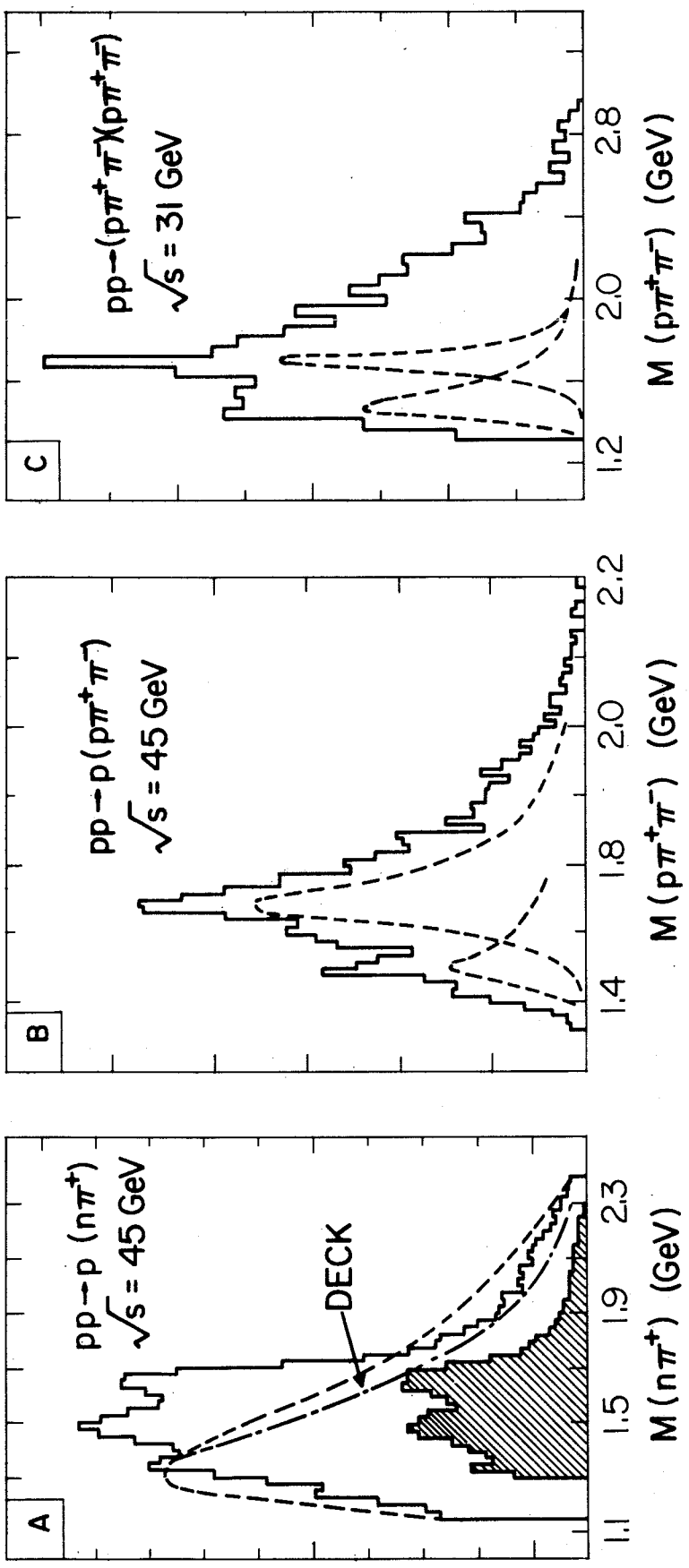

Figure 21 Invariant mass spectra for proton dissociation at the CERN ISR.

(A) $n\pi^+$ mass spectrum from ref. 108. The lines are the result of a Deck model calculation explained in subsection 5.4.

(B) $p\pi^+\pi^-$ mass spectrum from ref. 109.

(C) $p\pi^+\pi^-$ mass spectrum observed in double diffraction dissociation (110). The dashed lines in (B) and (C) represent resonance contributions.

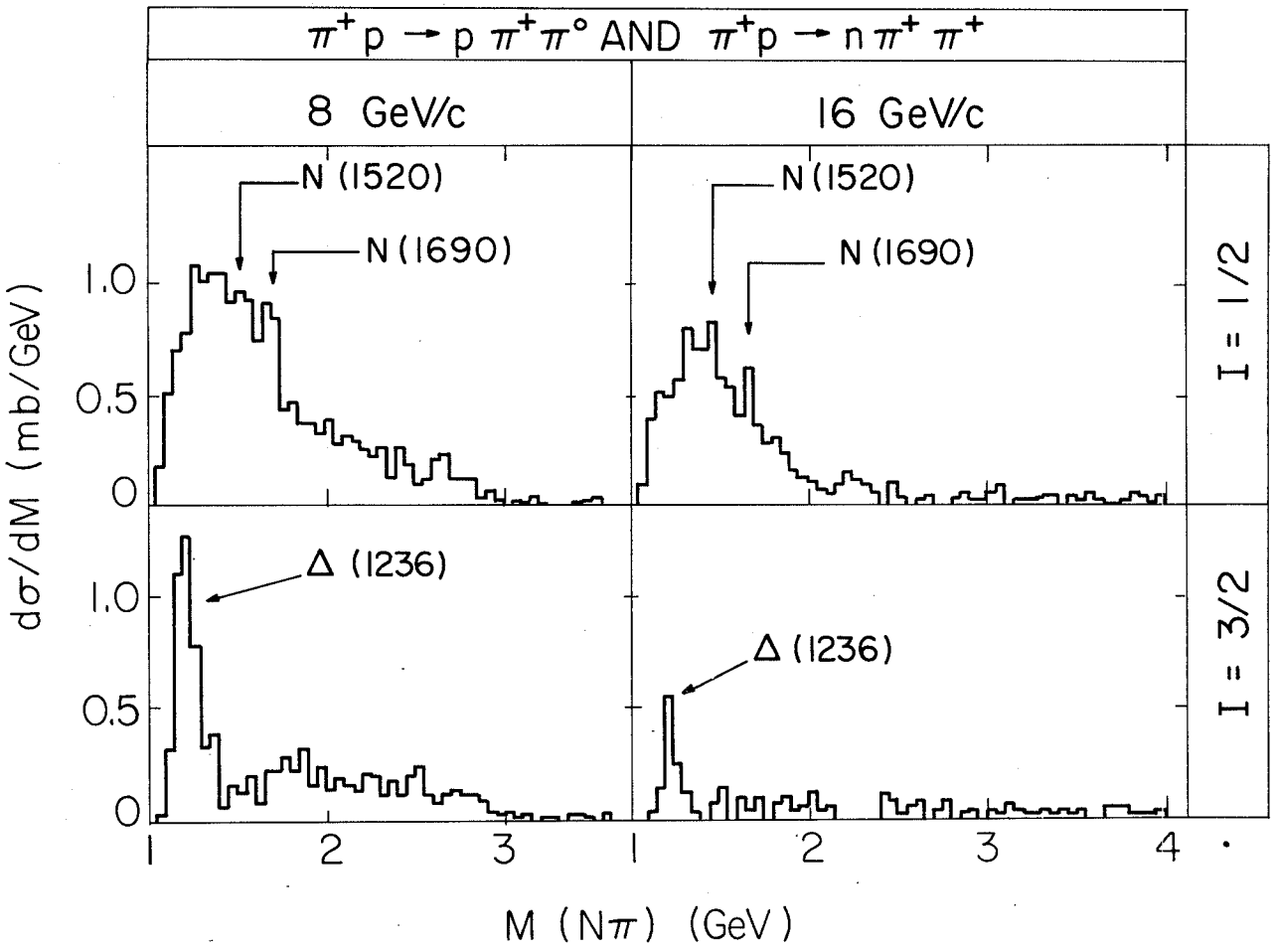

Figure 22 Results of isospin decomposition of the Nπ system produced in π^+p interactions at 8 and 16 GeV/c (111).

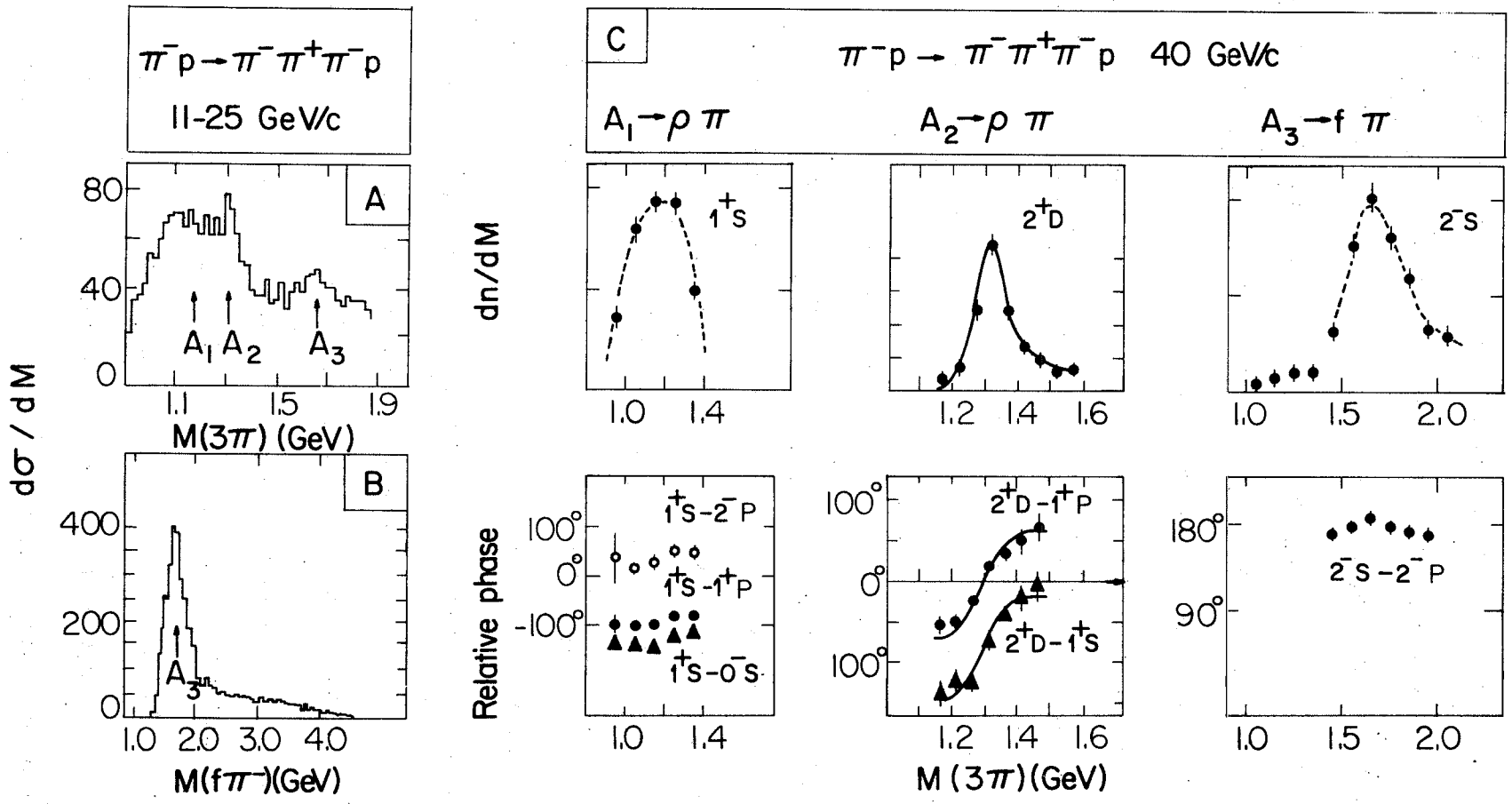

Figure 23 (A) $\pi^+\pi^-\pi^-$ mass spectrum from a world compilation of bubble chamber data (113).

(B) $f\pi^-$ mass distribution (113)

(C) Results of spin-parity analysis for the A_1, A_2 and A_3. The mass distribution of the dominant spin-parity state is shown together with relative phases (115).

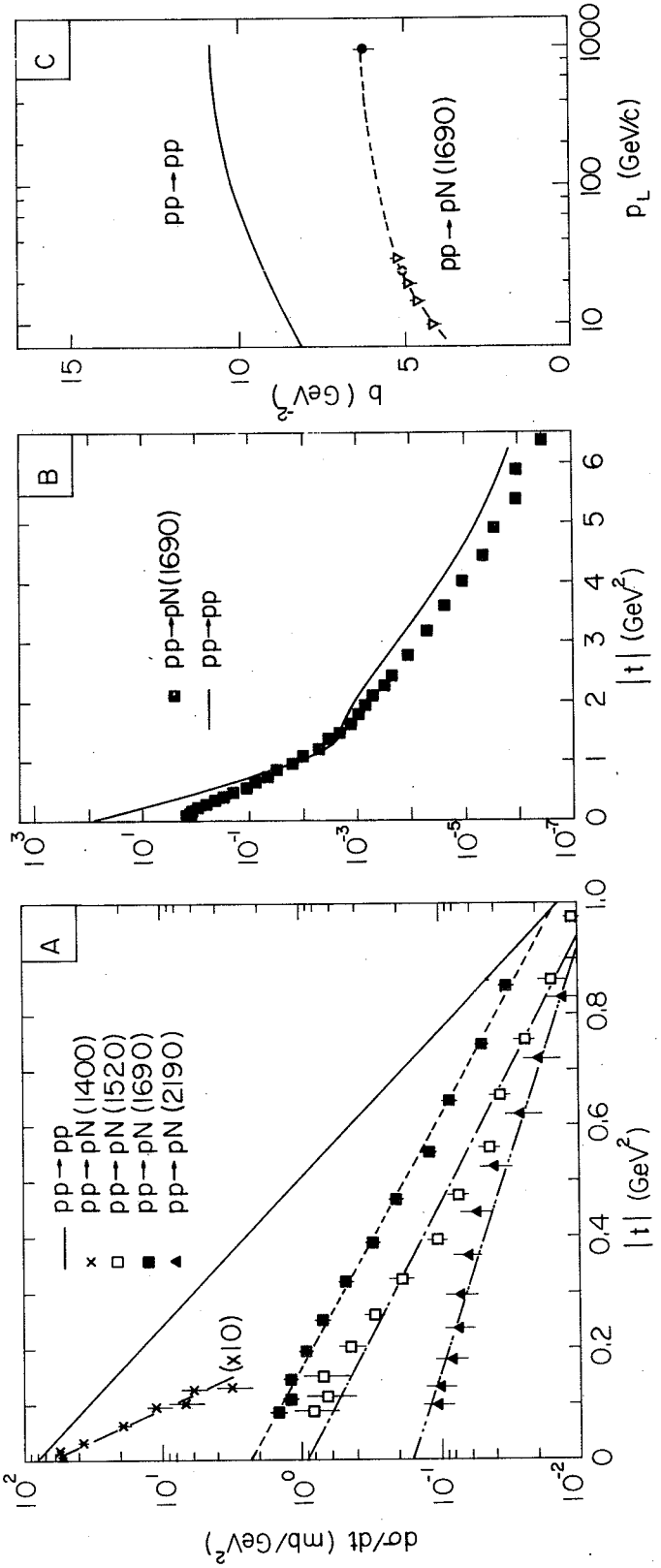

Figure 25 (A), (B) Momentum transfer distributions of the exclusive reactions pp → pN* at 24 GeV/c (78b). (C) Compilation of the forward slope b for the reaction pp → pN(1690) as a function of energy (47, 78b, 109). The continuous curve represents the elastic slope.

correlation is clearly present between the slope parameter b, describing the low t-region, and the mass of the $(n\pi^+)$ system.

Concerning the large t-region, outside the diffraction peak, only data at low-energy are now available. The differential cross-section for the reaction $pp \to pN(1690)$ measured by the CERN-Rome collaboration (78b) up to large momentum transfer ($-t \simeq 6$ GeV^2) is compared in Figure 25B with the shape of the elastic cross-section. As shown in Figure 13, at low energies proton-proton elastic scattering starts to develop a structure which at ISR energies eventually becomes a very clear diffractive-like minimum. The shape of the momentum transfer distribution for the reaction $pp \to pN(1690)$ at large t closely follows that of the elastic scattering distribution, providing evidence for a common, diffractive, mechanism. Some evidence also exists for a shrinking of the forward peak in the process $pp \to pN(1690)$, in close analogy with the well-known shrinking of the elastic peak, as shown in Figure 25C where data (47,78b) at AGS-PS energies are compared to a recent ISR result(109).

The energy dependence of the total cross-section for the two-body reactions $pp \to pN^*$ has been studied over a very wide energy range. The present experimental situation is illustrated in Figure 27 where data on the diffractive processes with excitation of the N(1400), N(1520) and N(1690) states are reported together with those referring to the reaction $pp \to p\Delta^+(1236)$, which involves change of isospin. The difference in energy dependence for the $I = \frac{1}{2}$ states, all of which satisfy the Gribov-Morrison rule, and the $I = 3/2$ resonance is striking.

The energy dependence of two-body inelastic reactions is customarily represented by means of the power law $\sigma \propto 1/p_L^n$ (49). This is not just a convenient way of parametrizing the data. In fact in the Regge picture if the exchange of only one trajectory dominates, then the energy dependence

In subsection 4.2 factorization in diffraction was presented as a characteristic feature of the exchange picture, i.e. of the fact that the Pomeron pole dominates in the t-channel. This kind of factorization does not arise naturally from an s-channel point of view (142), and at this stage experimental checks of its validity could be considered as supporting the fact that diffraction is better described by a factorizing Regge singularity. This statement is, however, incorrect. Since many years it has been known that factorization tests at the 10-20% level are not conclusive if they refer to the full cross sections (135). This has been checked explicitly in various simple optical models. For instance, the collision of two hadrons of different radii made up of a not too large number of constituents (partons) was considered by Fishbane and Trefil (143). In this case Glauber theory predicts factorization to better than 20%, almost independently of the value of the parton-parton cross-section, if the ratios of the radii and of the numbers of constituents of the two hadrons is within the range $1/3$ to 3. Similar conclusions are reached with other models. It even follows if hadrons are billiard balls the radii of which are chosen to reproduce the observed total cross-sections (144). These arguments show that factorization tests, to be really meaningful, should be performed on the differential cross-sections at the level of precision of a few percent. The rising total cross sections, which exclude the association of the Pomeron with a simple pole, leads us to expect approximate factorization anyway. Concluding we may say that approximate factorization appears as a general property of diffractive excitation . It may be used to predict at the 10-20% level the value of yet unmeasured cross-sections.

in Figure 32A. The rapidity distribution of the final state particles, represented by bars drawn at the corresponding rapidities, exhibit a gap between the rapidity of the quasi elastically scattered proton, which is very close to that of the incident proton, and those of all other particles. This is very different from what is now known to prevail for a typical many particle configuration, with the full rapidity interval rather uniformly populated. A quasi elastically scattered proton imposes such a rapidity gap. In effect, the secondaries resulting from the dissociation of an incident particle into a system of mass M appear on the rapidity plot as an elongated cluster centered at $y \approx \ln (s/M^2)/2$. The overall rapidity difference between the cluster and the quasi-elastically scattered proton is about $\ln(s/Mm)$, where m is the proton mass. However, even an isotopic cluster spreads out over at least two units of rapidity and thus, ascertaining the presence of a rapidity gap, does indeed require a high incident energy.

The kinematical configuration indicated in figure 32A is then much more clearly identified at ISR energies, where the global rapidity interval covers 8 units, than it is at AGS-PS energies, where it spans only 4 units. The occurrence of a large rapidity gap is readily associated with dominant Pomeron exchange, as depicted in figure 32A'. The larger the rapidity gap, the more important is Pomeron exchange as opposed to other exchange processes. Contributions from normal Regge trajectories are also present. However, once M is fixed, only Pomeron exchange will eventually remain at asymptotic energies.

Before discussing present experimental data on single diffraction dissociation, we briefly mention two other important diffractive processes.

The first one is double diffractive dissociation. A typical corresponding rapidity distribution is shown in figure 32B. A large rapidity gap separates the clustered distributions associated with the fragmentation of both diffractively excited protons. As mentioned in subsection 5.2, this process has been studied at the ISR only for the special case in which the protons are excited into rather low mass states(110). No data are available at present on double diffraction dissociation into large mass states, a process that could be studied only with high difficulties at the ISR,even taking advantage of the large rapidity range which is available.

The second, presently very interesting diffractive process,is double Pomeron exchange (Figure 32C'). The corresponding kinematical configuration now shows two rapidity gaps as illustrated in Figure 32C. This process is highly topical, as a diffractive process with no straightforward optical analogy while having a predictable cross section in terms of the exchange picture of diffraction. It will therefore be discussed at some length in section 7.

Focussing now on single diffraction dissociation (reaction 47), we recall that, for any inclusive reaction two different sets of variables are commonly used. They are either the longitudinal and transverse component of momentum, p_l and p_T respectively, of the quasi-elastically scattered proton or the four-momentum transfer squared t and the invariant mass squared M of the producted system X. As usual, $x = 2p_l/s^{\frac{1}{2}}$. At very large energies and for x close to one, the following relations hold

$$M^2 \approx s(1-x), \quad t \approx -p_T^2/x \ . \qquad 48.$$

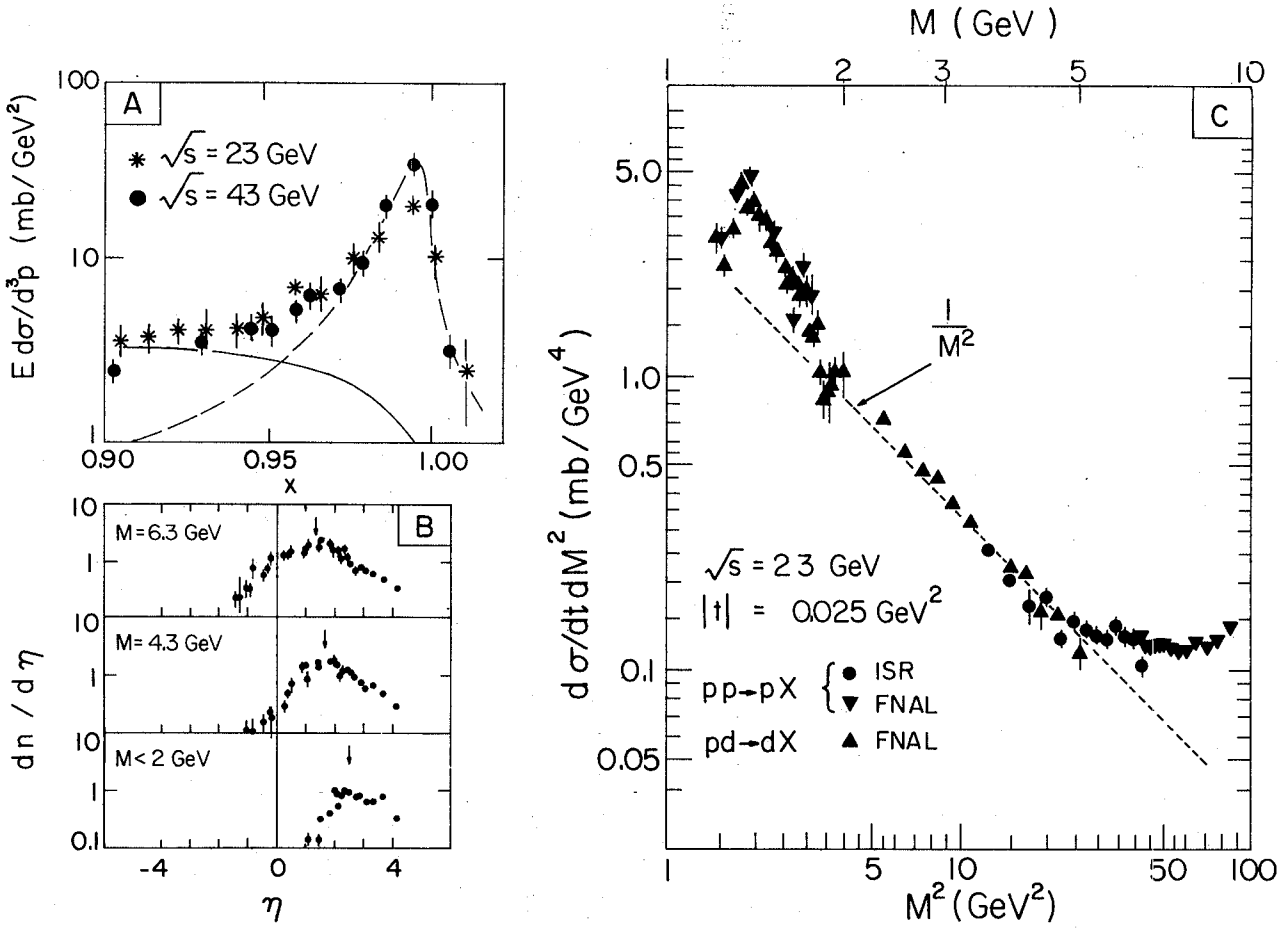

Figure 33 (A) ISR data (145) showing the x distribution of quasi-elastically scattered protons at p_t = 0.525 GeV/c.

(B) "Pseudo-rapidity" distribution resulting from the fragmentation of large mass M systems diffractively produced (149). The arrows indicate the centre of the distribution as expected from kinematics.

(C) Compilation of data (46) on M^2 dependence at fixed s and t.

The momentum transfer distribution in the region of the quasi-elastic peak has been extensively studied at FNAL and ISR. As an example we display in figure 34A t-distributions for two different values of M, measured at the ISR (151). These data were fitted by means of the function $\exp(bt + ct^2)$ in order to reproduce the curvature at large t.

We close this section with the following remark. If the inclusive cross section in the region of the diffractive peak actually scales with energy and if the diffractive production cross section at fixed mass is energy independent, two properties which are suggested by present data, then by integrating the $1/M^2$ distribution up to a fixed x value, which corresponds to a limiting value of M^2 increasing as s, the total diffraction cross section σ_D should increase logarithmically with energy. Values of σ_D estimated by the CERN-Holland-Lancaster-Manchester collaboration (151) are shown in figure 34B together with the trend of σ_{el}. While it is a definite experimental results that σ_D is comparable in magnitude to the elastic cross section σ_{el} ($\approx$ 7-8 mb), no definite statement can be made at present about the energy dependence.

From the measured value of σ_D, one can estimate the magnitude of the double diffraction dissociation cross section σ_{DD}, by using the factorization property $\sigma_{DD}\sigma_{el} = \sigma_D^2/4$. The value $\sigma_{DD} \approx 2$ mb is thus obtained.

5.7 Diffractive Effects in Photoproduction

There are great similarities between photoproduction and meson scattering. This is due to the fact that the relative weakness of the

electromagnetic coupling notwithstanding, the key features of the reaction are determined by the strong interactions of the hadrons which one finds in the final state. Regge models developed to describe the high-energy behaviour of hadron-hadron scattering have been extended to meson photoproduction . The cross section for the photoproduction of an exclusive final state (say, $\gamma p \rightarrow \pi^+ n$) typically decreases with energy according to the relevant exchanged Regge trajectory. Of special interest in the context of diffraction scattering is the photoproduction of those mesons which have quantum numbers identical to those of the photon (spin 1, negative parity, odd under charge conjugation). In addition to the well-known vector mesons ρ ,ω and ϕ, the recently discovered J/ψ and ψ' resonances satisfy those requirements.

The photoproduction of vector mesons is usually described by the graph of figure 35A whereby the photon switches into a vector meson which diffractively scatters off the target. Because of the diffractive nature of high-energy meson-nucleon scattering we expect the photoproduction of vector mesons to exhibit typical diffractive-like behaviour.

In the vector meson dominance model a direct coupling, described by the parameter γ_V, is introduced between the photon and the vector meson fields(152).This coupling can be expressed in terms of the partial width Γ_e for decay of the vector meson into a lepton pair (e^+e^- or $\mu^+\mu^-$) as

$$\Gamma_e = \frac{\alpha^2}{12} \left(\frac{4\pi}{\gamma_V{}^2} \right) M_V \qquad 50.$$

where α is the fine structure constant and M_V is the vector meson mass. The partial width Γ_e has been determined experimentally in two ways, by

measuring directly the branching ratio Γ_e/Γ_{tot} of vector mesons produced in hadronic interactions, and by measuring the total cross section of the process $e^+e^- \rightarrow$ vector meson at the e^+e^- colliding beams machines.

From the graph of figure 35A one may express the cross section for photoproduction of vector mesons off nucleons, in terms of the elastic vector meson-nucleon scattering as

$$\sigma(\gamma N \rightarrow VN) = \frac{\alpha}{4} \left(\frac{\gamma_V}{4\pi}\right)^{-1} \sigma(VN \rightarrow VN) \qquad 51.$$

if we accept to neglect off shell effects.

The elastic cross section $\sigma(VN \rightarrow VN)$ can be written in terms of the vector meson-nucleon total cross section $\sigma_t(VN)$ and of the slope b, using the optical theorem and the simplifying assumption that the elastic amplitude is purely imaginary, which should hold at high energy

$$\sigma(VN \rightarrow VN) = \frac{1}{16\pi b} \sigma_t^2(VN) \qquad 52.$$

By inserting eq.(52) in the expression (51) one may derive the vector meson-nucleon total cross section from photoproduction experiments, once γ_V is known.

Clearly a photoproduction cross section constant or slowly varying with energy implies a similar trend for the vector meson-nucleon cross section.

A compilation of data on $\rho^o p$ and ϕp total cross sections from Barger and Phillips(153a)is shown in figure 35B. These cross section values are typical of hadronic interactions and show a weak energy dependence. In figure 35C present results concerning the $J/\psi(3100)$-nucleon cross section are reported (153b). This cross-section quickly rises above threshold reaching a plateau at the level of about 1 mb. The sharp rise and

jet model and on the parton model where discussed by Bialas and Kotanski and by Resnick (156). However progress in this field is slow and this should not surprise given the difficulties encountered in computing even the much simpler elastic shadow.

In connection with elastic unitarity (equation 45), a much discussed problem concerns the diffractive contribution $G_D(a)$ to the inelastic overlap function $G_{in}(a)$. Going back to the Good and Walker approach (subsection 2.4), it is possible to derive an interesting bound on $G_D(a)$ (157). This bound is based on the hypothesis that diffractively produced states are physically distinguishable from pionization states, so that they do not interfere. The physical diffractive states $|h\rangle$ so defined may be decomposed in diffractive eigenstates $|n\rangle$, which by definition are not mixed by the interaction. Their profile functions $\Gamma_n(a)$, are supposed to be real. The profile function of the transition $|i\rangle \to |f\rangle$ (where $|i\rangle = \Sigma C_{ni}|n\rangle$ and $|f\rangle = \Sigma C_{nf}|n\rangle$) is simply $\Gamma_{fi} = \sum_n C^*_{nf}\Gamma_n C_{ni}$. Note that the C's form a unitary matrix. The elastic overlap integral is $\Gamma = \Sigma|C_{ni}|^2\Gamma_n$ and its contribution to the unitarity condition 45 is $|\Gamma|^2$. The contribution to the same equation of <u>all</u> diffractive final states is $\sum_f|\Gamma_{fi}|^2 = \Sigma|C_{ni}|^2\Gamma_n^2$. Since it comprises also the elastic contribution, to obtain the contribution of the diffractive final states one must subtract Γ^2:

$$G_D(a) = \sum_n|C_{ni}|^2\Gamma_n^2 - \Gamma^2 \leq \sum_n|C_{ni}|^2\Gamma_n - \Gamma^2 = \Gamma(a) - \Gamma^2(a) \qquad 53.$$

The inequality needed to obtain the Pumplin bound follows from the condition $\Gamma_n \leq 1$, which expresses probability conservation for the

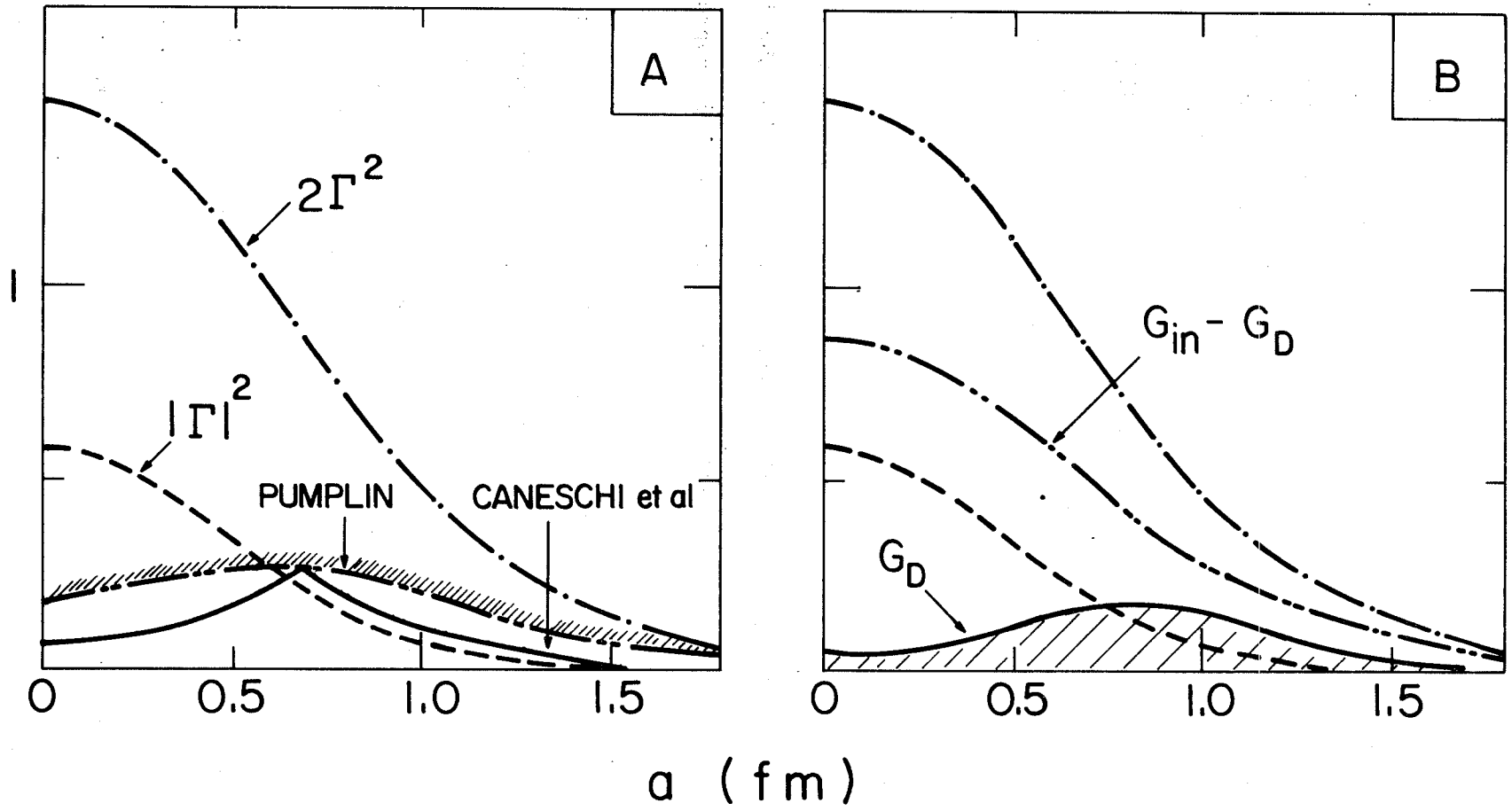

Figure 36 Impact parameter description of proton-proton scattering at 1480 GeV/c.

(A) The contributions to elastic unitarity are plotted together with the bounds due to Pumplin (157) and to Caneschi et al. (158) on the diffractive contribution G_D.

(B) The shaded area represents the diffractive overlap integral as computed by Sakai and White (159).

to handle all multiperipheral production amplitudes of the class of diagrams corresponding to Figure 37A. The corresponding shadow effect can in principle be calculated. However, the class of diagrams corresponding to Figure 37B, so far neglected, is different and yet interfers fully with that of Figure 37A. Taking it into accoun one can modify in an important way whatever shadow effect was previously calculated. Despite much past effort to build up diffraction from inelastic amplitudes (160a), no general and satisfactory prescription is presently available. Nevertheless, it remains that, in the framework of some simple field theories, such as ϕ^3 theory, the study of multiperipheral contributions to production amplitudes leads to an asymptotic energy behaviour for the elastic scattering amplitude which is associated with a (Pomeron) Regge pole (160b). Such a constructed Regge pole contribution is the shadow effect associated with a certain class of Feynman diagrams, as calculable in a particular theory, even if is not yet the full blown Pomeron looked for. It may therefore look as an a priori valuable input for a further more involved approach, which would include so far neglected inelastic processes. At present, theoretical approaches to the Pomeron start from such a "bare Pomeron" input, which one takes from some underlying field theory. One attempts to generate from it a better approximation to the actual diffractive amplitude. Indeed, a simple Pomeron pole, appealing as it may be, is not enough. We mentioned already the actually complicated nature of the Pomeron, as it gradually imposed itself from a phenomenological Regge approach and in particular after the discovery or rising cross sections.

For these reasons present approaches, starting from a "bare Pomeron" as previously defined, try to achieve building a full Pomeron amplitude

which takes what one calls a scaling form:

$$F(s,t) = is\,(\ell ns)^{K}\, g\left[-t(\ell ns)^{\nu}\right], \qquad 54.$$

as opposed to the simple Regge pole form:

$$R(s,t) = i\beta(t)\,\eta(t)s\ \exp\{[\alpha(t)-1]\,\ell ns\}\,. \qquad 55.$$

Different approaches differ in their values for κ and ν and in their predictions for the function g. They nevertheless have the same global form 54 . The total cross section grows as $(\ell ns)^{K}$. The slope parameter grows as $(\ell ns)^{\nu}$. The impact parameter picture for the asymptotic form 54. with an exponential for g is rather simple. The overall opacity grows as $(\ell ns)^{K-\nu}$, while the range grows as $(\ell ns)^{K/2}$ (the slope as $(\ell ns)^{\nu}$). Conversaly, its angular momentum plane description is complicated, with poles and cuts in the general case. It is interesting in any case than an approach which starts from the Regge pole side eventually arives at an amplitude which is amenable to a <u>simple</u> optical model picture but complicated Regge picture.

At present, reaching an asymptotic expression of the type 54 form an input "bare Pomeron" is achieved in two main different ways. One uses an s-channel approach or a t-channel approach. What actually goes under such code names, which relates to the fact that particular attention is paid to unitarity constraints in either the s and t channel, varies with time and schools. At present, one may say that the first one typically provides model amplitudes which saturate the Froissart bound (κ=2) (93) while the second one flourishes under the name of Reggeon Calculus or Reggeon field theory (160a, 160c, 161).

is of course too crude. More sophisticated methods have been devised. The procedure thus followed are however similar in spirit. One typically uses unitarity relations which involve themselves diffractive as well as non diffractive amplitudes as a constraint on the input amplitude. The Pomeron contribution is then the solution of an integral equation. Various values for κ and ν result, depending on the bare Pomeron intercept and on the conditions required (164,165). The full Pomeron is always a complicated object. One may get theoretically satisfactory asymptotic amplitude. However, the proton-proton profile function observed at ISR energies is very far from a black disc, and models of this type are certainly not applicable in this energy region.

6.3 The t-channel Approach

The t-channel approach is of particular interest at present since it relies on topical developments in field theory. Again one tries to achieve a richer amplitude from a Regge pole input (160,161). The first step is to translate the rules for Regge exchange (160), as obtained in an underlaying field theory as ϕ^3 theory, into those of a field theory in two space and one time dimension where the two-momentum k is such that $-k^2 = t$ and the energy is $1 - \alpha(t)$. The Lagrangian contains a free term expressed in terms of the Pomeron field operator and a coupling term for which one finds good reason to limit oneself to a triple Pomeran coupling. In this approach, one takes into account interactions among input Pomeron - as they may enter unitary from the t-channel point of view - as apposed to the multiple exchange of input Pomeron among scattering particles, which enters unitarity in the s-channel.

The Regge calculus approach is however very far from having been fully explored and interesting developments should be expected. Other types of Lagrangian, with bare Pomeron originating from other types of underlaying field theory can be considered. We can but refer the reader to ref. 161.

A conclusion at the present time is not possible. Rising cross sections have required asymptotic forms for the diffractive amplitude which are well within reach of available theoretical models. However, the basic property, the fact that up to logarithms, cross sections are apparently constant has to be put into the theory. It does not follow, as one would certainly wish, from some fundamental property. At the same time, if cross section can rise within present models, there is no understanding why they rise so little. Within the ISR energy range, the s-channel approach would find it more natural to see the proton cross section rise hundred times faster (full absorption) whereas the t-channel approach provides an acceptable asymptotic expression but with values of K and ν which have no reason to apply to present data. It should apply only for large values of ℓns! What we see in present experiments is still very different from the output Pomeron arrived at. How much it resembles to a simple input Pomeron is unclear, yet we hope that this section will have convinced the reader that the question is very much alive.

7. DIFFRACTION EXCITATION SEEN AS POMERON EXCHANGE

7.1 The Triple Regge Formalism

As discussed in subsection 5.6, single diffractive excitation corresponds to an important and already rather well explored inelastic mechanism. Its

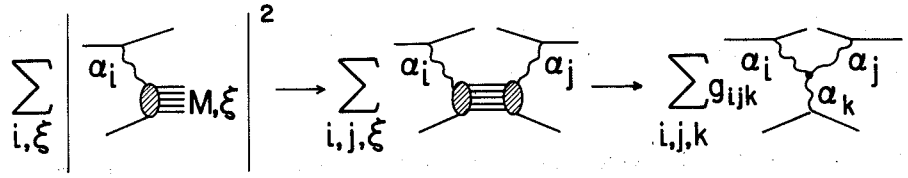

Figure 38 Schematic calculation of the inclusive distribution in the triple-Regge formalism. A Regge approximation is used for the absorptive part of the Reggeon proton elastic amplitude.

the presence of s/M^2 translates only the scaling large s and large M^2 behaviour. Extra constant terms could also have been included with a correlated change in σ_p. We should therefore only stress that the Pomeron-proton cross section, after a sharp drop with increasing M^2, corresponding to the faster than M^2 fall in **Figure 33C, practically levels for $M^2 > 5$ GeV^2.** It shows a typical hadronic behaviour and typical hadronic value.

The triple Regge formmalism is also useful at isolating special kinematical dependences, such as those outlined in fig. 33A, relating them to specific Reggeon exchanges. One may for instance limit oneself to Pomeron P with intercept[1] and secondary Reggeon R with typical intercept $\frac{1}{2}$, and to symmetric terms $i \equiv j$. The energy behaviour of the inclusive cross section, together with its mass and x **dependences, are then summarized** for small t in Table 5.

It is therefore Pomeron exchange dominance in the Reggeon-proton amplitude which is connected with the scaling property of the quasi-elastic peak ($\alpha_k(0) = 1$), whether we deal with Pomeron exchange (diffraction) or secondary reggeon exchange (standard type of **process) in the first place.** With the PPP and RRP contributions we respectively obtain the dashed and solid curves of **Figure 33A.**

7.2 The Pomeron-proton Interaction

Continuing in our analysis of diffraction in terms of a Pomeron-proton interaction, next to the total Pomeron-proton cross section comes the inclusive distribution of the fragments of the excited proton. As previously said, when of a low invariant mass they are separated from the quasi

elastically scattered proton by a large rapidity gap and they cluster over two units of rapidity. As the mass increases, however, they fill the kinematically available rapidity interval, which increases as $\ell n\ M^2$. The inclusive distributions, as shown in **Figure 33B, exhibits a rise of the** rapidity distribution at maximum with increasing M^2, as the maximum shift towards the center. It could eventually level off. The key point, however, is the spread of the rapidity distribution with increasing M^2. It is compatible with $\ell n\ M^2$. Indeed, the proton fragments fill all of their kinematically allowed rapidity range which as previously discussed, increases as $\ell n\ M^2$. All this is extremely similar to what observed in hadron-hadron collisions. As already remarked, also the associated charged multiplicity (the integral over the rapidity distributions in **Figure 33B)** compares well with what observed in hadron-hadron collisions at $\sqrt{s} = M$.

The kinematical spread of the secondaries has a striking effect when analyzed in terms of the full CM rapidity. The centre of mass of the hadronic system of mass M shifts towards rapidity zero by an amount $\ell n\ M$ from the incident proton rapidity $\ell n\ \sqrt{s}$. However, since secondaries are spread over a $\ell n\ M$ segment on either side of their centre of mass rapidity value, fragments still reach the boundary of the rapidity interval whatever M is. This is compatible with **Figure 33B. The use of pseudo rapidity may** however somewhat smear whatever is actually occuring at the kinematical boundary. At present there are many open questions which call for more data. The inclusive distribution may well not be symmetric at presently accessible masses but show some skewness favouring the Pomeron side, in much the same way as what is observed in photoproduction. Data are compatible with that but certainly not accurate enough yet. The inclusive

special distribution of Figure 32C. There is of course no reason why the protons could not flare as well. Yet, in order to maximize the rapidity gaps so that double Pomeron exchange could be favoured, one is presently led to focuse on processes where the two protons are merely quasi-elastically scattered (with $x > 0.96$) and a few slow centre of mass particles (typically a $\pi^+\pi^-$ system) are also produced.

The Pomeron exchange picture of diffractive excitation calls for the occurence of such a process with, in principle, a predictable cross section, estimate for which are at the 10-20 μb level. The kinematics of the process simplify in the asymptotic limit (large s/s_1 and s/s_2, large s_1 and s_2, and large M^2, using the notations spelled out by Figure 32C'). There are then two large rapidity gaps

$$Z_1 = \ell n\ s/s_1, \quad Z_2 = \ell n\ s/s_2 \qquad 63.$$

and

$$M^2 = s_1 s_2/s. \qquad 64.$$

To the extent that the four units of rapidity available at PS (AGS) energies are enough to get strong evidence for single diffractive excitation, one may hope that the eight units available at the ISR could be enough to secure evidence for double Pomeron exchange. Background problems may however be very important. Furthermore, even at ISR energies, two large enough rapidity gaps ($Z > 3$ say) can be achieved only at the expense of taking a rather small M^2. Despite all that it remains that double Pomeron exchange has a particular interest in that the optical picture, which can be advocated for single and double diffraction, no longer readily applies. We have rather to deal with the hadronic polarization of the vacuum, following a process which the Pomeron exchange picture of diffraction imposes. It is then worth searching for.

$$\frac{x_1 x_2 \, d^2\tilde{\sigma}}{dx_1 \, dp_{T_1}^2 \, dx_2 \, dp_{T_2}^2} = \frac{x_1 \, d\tilde{\sigma}}{dx_1 \, dp_{T_1}^2} \, \frac{x_2 \, d\tilde{\sigma}}{dx_2 \, dp_{T_2}^2} \, \frac{1}{\tilde{\sigma}_t} \, . \qquad 67.$$

The twidle sign on top of the σ's are here to warn again that the relation applies only to the Pomeron contribution, to double Pomeron exchange on the left hand side, and single Pomeron exchange on the right hand side. What belongs to Pomeron exchange (large M^2 limit) in single diffractive excitation is however not precisely known yet (174). For these reasons one may give only an order of magnitude estimate for the expected double Pomeron exchange contribution in the large M^2 limit. As anticipated, it is at the 10 μb level.

In the low M^2 region, with typically a two-pion state produced, one may attempt a different estimate based on pion exchange in the central blob (172,173). The expected cross section has the same order of magnitude. It is low for a background with hadronic process, but large enough to be seen. The main question is of course the practical separation of the double Pomeron contribution associated with expression 65, from background terms, the main one being the large mass low multiplicity tail of single diffraction excitation which could overcome the looked for signal.

It is usually stressed that the double Pomeron contribution is the only one to include a double pole term as x_1 and x_2 approach one. Indeed, relation 65, written for $\alpha(t) \tilde{\sim} 1$ gives

$$\frac{d\sigma}{dx_1 \, dx_2} \sim \frac{1}{(1-x_1)(1-x_2)} \, , \qquad 68.$$

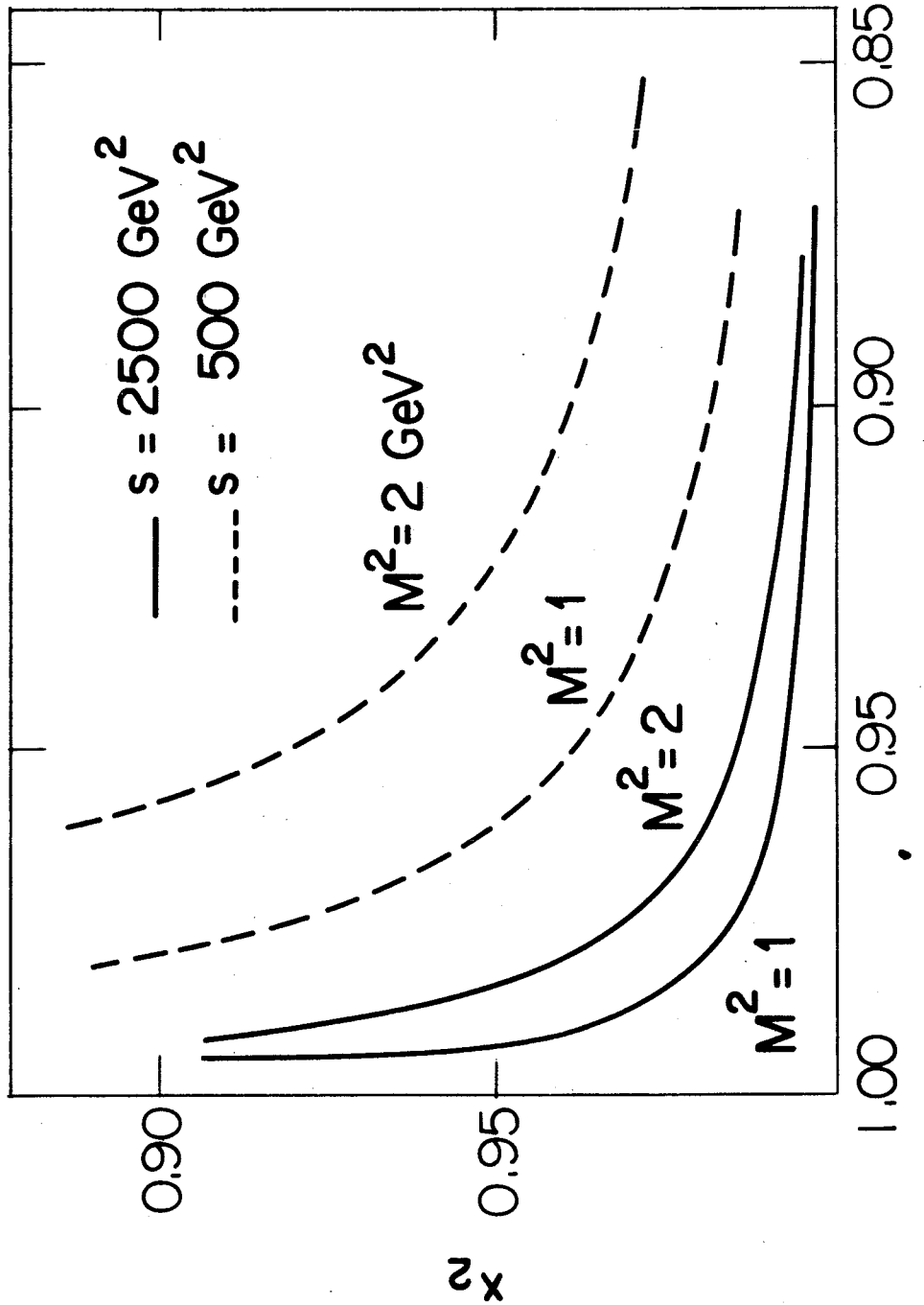

Figure 39 Kinematical domain available for double-Pomeron exchange at fixed invariant mass. The kinematical separation of the process may require x values as large as 0.96. Even at ISR energies one is limited to low-mass values.

involved, simplicity would prevail. Rising cross-sections over the ISR energy range have shown that nothing seems to stabilize. Asymptopia was but an elusive concept! If present theories can easily accommodate rising cross-sections, we have yet no explanation for the slow pace at which they grow. The Pomeron is now expected to be a complicated object at extremely high energies, but we have as yet no satisfactory explanation for the fact that it is empirically so simple at present energies. It was also usually assumed that diffraction excitation was a relatively unimportant phenomenon limited to low mass hadronic states. It now appears as a very sizeable effect cross-section wise and there seems to be no bound on the mass of the diffractively excited object, provided the energy is high enough. When translating it easily in the framework of the triple-Regge analysis, one partly eludes what it means in terms of the hadron structure.

There are many questions which should be explored experimentally better than they are at present. Does the elastic peak shrink at large momentum transfer? Are diffractive cross-sections, for specific final states, constant over the ISR energy range? What are the correlations among the many particles into which a large mass diffractively excited system resolves itself?

These are merely a few among many. The existence or not of double-Pomeron processes is also a very topical question in view of it being characteristic of the exchange picture of diffraction much more than any of the other processes.

The diffraction of hadronic waves is a very interesting facet of particle physics. It is simple by the basic concepts it uses, and rewarding by the many phenomena it correlates.

REFERENCES

1. Van Hove, L. 1967. In High Energy Physics and Nuclear Structure, ed. G. Alexander, 259-273. Amsterdam: North Holland.

2. Gottfried, K. 1972. Optical Concepts in High Energy Physics. CERN 72-20. 21 pp.

3. Cocconi, G. 1973. Proc. R. Soc. Lond. A 335: 409.

4. Perl, M.L. 1974. High Energy Hadron Physics. New York: Wiley

5. Born, M., Wolf, E. 1972. Principles of Optics. Oxford: Pergamon Press.

6. Überall, H. 1971. Electron Scattering from Complex Nuclei. New York: Academic Press

7. Alkhazov, G.D. et al. 1975. Phys. Lett. B 57: 47.

8. Bertini, R. et al. 1973. Phys. Lett. B 45: 119.

9. Böhm, A. et al. 1974. Phys. Lett. B 49: 491

10. Auger, J.P. Lombard, R.J. 1973. Phys. Lett. B 45: 115.

11a. Böhm, A. et al. 1974. Phys. Lett. B 49: 491.

11b. Kac, M. 1973. Nucl. Phys. B 62: 402.

12. Glauber, R.J. 1955. Phys. Rev. 99: 1515.

13. Feinberg, E.L., Pomeranchuk, I. Ia. 1956. Supp. Nuovo Cimento 3: 652.

14. Good, M.L., Walker, W.D. 1960. Phys. Rev. 120: 1857

15. Bemporad, C. et al. 1971. Nucl. Phys. B 33: 397.

16. Bemporad, C. et al. 1972. Nucl. Phys. B 42: 627

17. Mühlemann, P. et al. 1973. Nucl. Phys. B 59: 106

18. Beusch, W. et al. 1975. Phys. Lett. B 55: 97

19. Beusch, W. 1972. Acta Phys. Polonica B 3: 679

20. Bellini G. 1975. In Proc. of the Topical Meeting on High Energy Collisions Involving Nuclei, ed. G. Bellini et al. 317. Bologna: Compositori

21. Glauber, R.J. 1959. In Lectures in Theoretical Physics, ed. W.E. Brittin et al. 1: 315. New York: Interscience.

44. Akimov, Y. et al. 1975. Phys. Rev. Lett. 35: 763.

45. Akimov, Y. et al. 1975. Phys. Rev. Lett. 35: 766

46. Melissinos, A.C., Olsen, S.L. 1975. Phys. Rep. C 17: 77-132.

47. Edelstein, R.M. et al. 1972. Phys. Rev. D. 5: 1073.

48. Gribov, V.N. 1967. Yadernaya Fiz. 5: 197.

49. Morrison, D.R.O. 1968. Phys. Rev. 165: 1699.

50. Goldhaber, A., Goldhaber, M. 1966. In Preludes in Theoretical Physics, in honour of V.F. Weisskopf, ed. A. de Shalit et al., 313. Amsterdam: North Holland.

51. Kölbig, K.S., Margolis, B. 1968. Nucl. Phys. B 6: 85.

52. Gobbi, B. et al. 1974. Coherent Proton Dissociation on Nuclear Targets. Unpublished.

53. Rogers, C., Wilkin, C. 1972. Nucl. Phys. B 45: 47

54. Van Hove, L. 1972. Nucl. Phys. B 46: 75

55. Gottfried, K. 1972. Acta Physica Polonica B 3: 769.

56. Voyvodic, L. 1976. Phys. Report C, To be published.

57a. Ting, S.C.C. 1968. In Proc. of the XIV Int. Conf. on High Energy Phys., Vienna. ed. J. Prentki and J. Steinberger. 43. Geneva: CERN.

57b. Ting, S.C.C. 1970. In Proceedings of the Topical Seminar on Interactions of Elementary Particles with Nuclei, ed. G. Bellini et al. Trieste: INFN.

58. Silverman, A. 1975. Review of High Energy Photoproduction. In Proc. of the 7th Int. Symposium on Lepton and Photon Interactions at High Energy. Stanford. August 1975.

59a. Wetherell, A.M. 1975. Elastic and Total Cross-Sections and Implications. In Proc. of the EPS Int. Conference on High Energy Physics. Palermo. June 1975.

59b. Galbraith, W. et al. 1965. Phys. Rev. B 138: 913.

59c. Foley, K.J. et al. 1967. Phys. Rev. Lett. 19: 857.

59d. Denisov, S.P. et al. 1973. Nucl. Phys. B 56: 1.

76. Borghini, M. et al. 1971. Phys. Lett. B 36: 493.

77. Gaidot, A. et al. 1975. Phys. Lett. B 57: 389.

78a. Clyde, A.R. 1966. University of Cal. Rad. Lab. Report. UCRL 16275.

78b. Allaby, J.V. et al. 1973. Nucl. Phys. B 52: 316.

78c. Akerlof, C.W. et al. 1975. Phys. Lett. B 59: 197.

78d. de Kerret, H. et al. 1976. Phys Lett. B. To be published.

79. Kwak, N. et al. 1975. Phys. Lett. B 58: 233.

80. Dias de Deus, J. 1973. Nucl. Phys. B 59: 231.

81. Berger, V. 1974. In Proc. of the 17th Int. Conf. on High Energy Physics, ed. J.R. Smith. 1: 200: Didcot, England: Rutherford Lab.

82a. Amaldi, U. et al. 1971. Phys. Lett. B 44: 116.

82b. Beznogikh, G.et al. 1973. Phys. Lett. B 43: 85.

82c. Bartenev, V. et al. 1973. Phys. Rev. Lett. 31: 1088.

82d. CERN-Rome Collaboration. 1976. Phys. Lett. To be published.

82e. Nurushev, S. 1974. In Proc. of 17th Int. Conf. on High Energy Physics. ed. J.R. Smith. 1 : 25. Didcot, England: Rutherford Lab.

82f. Derevchekov, A.A. et al. 1974. Phys. Lett. B 48: 367.

82g. Antipov, Yu.M. et al. 1973. Nucl. Phys. B 57: 333.

82i. Fermilab Single Arm Spectrometer Group 1975. Phys. Rev. Lett. 35: 1406

82j. Akerlof, C.W. et al. 1975. Phys. Rev. Lett. 35: 1406.

83. Amaldi, U. 1973. In Proc. II Int. Conf. on Elementary Particles (Aix-en-Provence) Jour. de Phys. 34C1: 241.

84. Barbiellini, G. et al. 1972. Phys. Lett. B 39: 663.

85. Grein, W., Kroll, P. 1975. Phys. Lett. B 58: 79.

86. Barger, V., Phillips, R.J.N. Rutherford Lab. Report RL75-176 T.145

87a. Carlson, P.J., Diddens, A.N., Giacomelli, G., Mönnig, F., Schopper, H. 1973. Landolt-Börnstein New Series. 1971. ed. K.H. Hellwege. Vol. 7. Berlin: Springer-Verlag

95k. Kirillova , L.F. et al. 1966. Zh. Eksperim i Teor. Fiz. 50: 76.

951. Beznogikh, G.G. et al. 1972. Phys. Lett. B 39: 411.

95m. Taylor, A.E. et al. 1965. Phys. Lett. 14: 54.

95n. Bartenev, V. et al. 1973. Phys. Rev. Lett. 31: 1367.

95o. Amaldi, U. et al. 1973. Phys. Lett B 43: 231.

95p. Hendrick, R.E., Lautrup, B. 1975. Phys. Rev. D 11: 529.

95q. Hendrick, R.E. et al. 1975. Phys. Rev. D 11:536.

96. Van Hove, L. 1964. Rev. Mod. Phys. 36: 657.

97a. Michejda, L. 1968. Nucl. Phys. B 4: 113.

97b. Koba, Z., Namiki M. 1968. Nucl. Phys. B 8: 413.

98a. Miettinen, H.I. 1973. In Proc. II Int. Conf. on Elementary Particles (Aix-en-Provence) Jour. de Phys. 34C1: 263.

98b. Miettinen, H.I. 1974. In Neuvième Rencontre de Moriond. Interactions Hadronique à Haute Energie. ed. J. Tran Thanh Van. 1: 363. Orsay: CNRS.

99. Hwa, R.C. 1973. Phys. Rev. D 8: 1331.

100. Hamer, C.J., Pierls, R.F. 1973. Phys. Rev. D 8:1358.

101. Heniey, F.S. 1973. Phys. Lett. B 45: 469.

102. Grein, W., Guigas, R., Kroll, P. 1975. Nucl. Phys. B 89: 93.

103a. Martin, A. 1975. Testing geometrical scaling. Unpublished.

103b. Berger, V., Luthe, J., Phillips, R.J.N. 1975. Test of Geometrical Scaling and Generalizations. Unpublished.

104. Van Hove, L., Fiatkowski K. 1976. TH 2133 - CERN.

105. Anderson, E.W. et al. 1970. Phys. Rev. Lett. 25: 699.

106. Morrison, D.R.O. 1974. In Neuvième Rencontre de Moriond. Interactions Hadroniques à Haute Energie. Ed. J. Tran Thanh Van. 1: 275. Orsay: CNRS.

107. Morrison, D.R.O. 1974. In Proc. of the Fifth Hawaii Topical Conference in Particle Physics , ed. P.N. Dobson et al. 189. Honolulu: Univ. Press of Hawaii.

108. Nagy, E. et al. 1976. Phys. Lett. B. To be published.

109. Webb, R. et al. 1975. Phys. Lett. B 55: 331.

131b. Cocconi, G. et al. 1961. Phys. Rev. Lett. 7: 450.

132. Berger, E.L. 1968. Phys. Rev. 166: 1525.

133. Miettinen, H.I., Pirilä, P. 1972. Phys. Lett. B 40: 127.

134. Berger, E.L., Pirilä, P. 1975. Phys. Lett. B 59: 361.

135. Freund, P.G.O. 1968. Phys. Rev. Lett. 21: 1375.

136. Beaupré, J.V. et al. 1973. Nucl. Phys. B 66: 93.

137. Graessler, H. et al. 1972. Nucl. Phys. B 47: 43.

138. Böckmann, K. et al. 1974. Nucl. Phys. B 81: 45.

139. Kittel, W., Ratti, S., Van Hove, L. 1971. Nucl. Phys. B 30: 333.

140. Liu, F.F. et al. 1972. SLAC-PUB-1057.

141. Cavalli-Sforza, M. 1975. Lett. Nuovo Cimento 14: 345.

142. Van Hove, L. 1971. Ann. Phys. 66: 449.

143. Fishbane, P.M., Trefil, J.S. 1974. Phys. Rev. Lett. 32: 396.

144. Pumplin, J., Kane, G.L. 1974. Phys. Rev. Lett. 32: 963.

145a. Albrow, M.G. et al. 1973. Nucl. Phys. B 51: 388.

145b. Albrow, M.G. et al. 1974. Nucl. Phys. B 72: 376.

146. Böggild, H., Ferbel, T. 1974. Ann. Rev. Nucl. Sci. 24: 451.

147. Whitmore, J., 1974. Phys. Rep. C 10: 273.

148. Slansky, R. 1974. Phys. Rep. C 11: 99.

149. Albrow, M.G. et al. 1974. Phys. Lett. B 51: 424.

150. Schamberger, R.D. et al. 1975. Phys. Rev. Lett. 34: 1121.

151. Albrow, M.G. et al. 1976. Nucl. Phys. To be published.

152. Sakurai, J.J. 1969. In Lecture in Theoretical Physics: Elementary Particle Physics, ed. K.T. Mahanthappa et al. 11A. New York: Gordon and Breach.

153a. Barger, V., Phillips, R.J.N. 1975. Nucl. Phys. B 97: 452.

153b. Barger, V., Phillips, R.J.N. 1975. Preprint Univ. of Wisconsin COO 881-462.